JGR Atmospheres

RESEARCH ARTICLE
10.1029/2023JD039270

Stratosphere-Troposphere Exchanges of Air Mass and Ozone Concentrations From ERA5 and MERRA2: Annual-Mean Climatology, Seasonal Cycle, and Interannual Variability

Mingcheng Wang[1], Qiang Fu[1], Anna Hall[1], and Aodhan Sweeney[1]

[1]Department of Atmospheric Sciences, University of Washington, Seattle, WA, USA

Key Points:

- Annual-mean global ozone stratosphere-troposphere exchanges (STEs) from ERA5 and Modern Era Retrospective analysis for Research and Application, version 2 (MERRA2) are 380 and 361 Tg year^{-1}, with difference mainly due to diabatic heating
- 40% (−40%) difference between ERA5 and MERRA2 in global ozone STEs in boreal summer (fall) is mainly due to lowermost stratosphere ozone mass change rate difference
- ERA5 and MERRA2 can only explain each other's variance in global ozone STE monthly anomalies by 33%, and the variance explained by Brewer-Dobson circulation is <5%

Supporting Information:

Supporting Information may be found in the online version of this article.

Correspondence to:

Q. Fu,
qfu@uw.edu

Citation:

Wang, M., Fu, Q., Hall, A., & Sweeney, A. (2023). Stratosphere-troposphere exchanges of air mass and ozone concentrations from ERA5 and MERRA2: Annual-mean climatology, seasonal cycle, and interannual variability. *Journal of Geophysical Research: Atmospheres*, *128*, e2023JD039270. https://doi.org/10.1029/2023JD039270

Received 18 MAY 2023
Accepted 28 NOV 2023

Abstract Stratosphere-Troposphere exchange (STE) of air mass and ozone in ERA5 and Modern Era Retrospective analysis for Research and Application, version 2 (MERRA2) reanalyses from 1980 to 2022 are investigated on their seasonal cycle, annual-mean climatology, and monthly anomalies smoothed using a 1-year Lanczos low-pass filter. We employ a lowermost stratosphere mass budget approach with dynamic isentropic surfaces fitted to tropical tropopause as the upper boundary of lowermost stratosphere. The annual-mean ozone STEs over the NH extratropics, SH extratropics, tropics, extratropics, and globe in ERA5 are −342, −239, 201, −581, and −380 Tg year^{-1}, respectively, versus −305, −224, 168, −529, −361 Tg year^{-1} from MERRA2. The annual-mean global ozone STE difference between ERA5 and MERRA2 is dominated by the diabatic heating difference, partly compensated by the ozone concentration difference. There are about 40% (−40%) differences between ERA5 and MERRA2 in global ozone STEs in boreal summer (autumn), mainly due to the difference in seasonal breathing of the lowermost stratosphere ozone mass between reanalyses. The correlation coefficient between ERA5 and MERRA2 global ozone mass STE monthly anomalies is 0.57 and thus ERA5 and MERRA2 can only explain each other's variance by 33%. Multiple linear regression analysis shows that El Niño–Southern Oscillation, quasi-biennial oscillation, and Brewer-Dobson circulation explain the variance in the ERA5 (MERRA2) global ozone STE monthly anomalies by 17.3 (5.0), 5.4 (7.2), and 1.0 (3.1)%, respectively. The volcanic aerosol impacts on ozone STEs from ERA5 and MERRA2 have opposite signs and thus are inconclusive. Cautions are therefore needed when using ERA5 and MERRA2 to investigate the STE seasonal cycle and interannual variability.

Plain Language Summary Stratosphere-troposphere exchange (STE) of ozone can impact surface ozone concentration and air quality. We investigate air mass and ozone STEs using two state-of-art and widely used reanalyses, that is, ERA5 and Modern Era Retrospective analysis for Research and Application, version 2 (MERRA2) from 1980 to 2022, on annual-mean climatology, seasonal cycle, and monthly anomalies. The magnitudes of annual-mean global ozone STEs in ERA5 and MERRA2 are 380 and 361 Tg year^{-1}, respectively. The relative differences between ERA5 and MERRA2 in global ozone STEs can be up to 40% (−40%) in boreal summer (autumn). In addition, we find the ERA5 and MERRA2 STE monthly anomalies are quite different: the correlation coefficient between ERA5 and MERRA2 global ozone STE monthly anomalies is only 0.57. We further investigate the impacts of climate variabilities and perturbations, including El Niño–Southern Oscillation, quasi-biennial oscillation, Brewer-Dobson circulation, solar cycle, and volcanic aerosols on the air mass and ozone STE interannual variabilities. We find that the Brewer-Dobson circulation can only explain very small variances in ERA5 and MERRA2 air mass and ozone STE monthly anomalies. We show that 67%–77% of the global ozone STE interannual variances from ERA5 and MERRA2 cannot be explained by the climate variabilities and perturbations considered.

1. Introduction

As an important source for the tropospheric ozone budget, stratosphere-troposphere exchange (STE) of ozone could substantially impact surface ozone concentrations and air quality (e.g., Lin et al., 2015; Ordonez et al., 2007). For example, using surface ozone measurements and a nudged chemistry-climate model, Lin et al. (2015) showed that surface ozone concentrations over the western US could be elevated to unhealthy levels by stratospheric ozone influx. In addition, the ozone STE could impact the tropospheric oxidation capacity and methane lifetime (e.g., Fiore et al., 2002; Geng et al., 2017; Kentarchos & Roelofs, 2003).

The reanalysis data have been widely used to investigate air mass and ozone STEs (e.g., Boothe & Homeyer, 2017; Gettelman et al., 1997; Olsen et al., 2013; Škerlak et al., 2014; Wang & Fu, 2021). For example, by applying the Lagrangian trajectory approach to the reanalysis fields, air mass and ozone STE transport pathways can be identified (e.g., Boothe & Homeyer, 2017; Škerlak et al., 2014; Stohl et al., 2003). Š;kerlak et al. (2014) estimated the global air mass and ozone STEs for 1979–2011 and quantified their geographical distribution and preferred transport pathways based on the ERA-Interim reanalysis. Boothe and Homeyer (2017) examined the global large-scale STEs from four modern reanalysis, including ERA-Interim, JRA-55, Modern Era Retrospective analysis for Research and Application (MERRA), and version 2 of this system (MERRA2). The lowermost stratosphere mass budget method (e.g., Appenzeller et al., 1996) is a powerful approach that is accurate to estimate the net fluxes of air, ozone, and other chemical species across the tropopause over the Northern Hemisphere (NH) extratropics, Southern Hemisphere (SH) extratropics, tropics, and globe (e.g., Gettelman et al., 1997; Olsen et al., 2013; Wang & Fu, 2021). Although the location and time of STE events cannot be isolated using the budget approach, the estimates obtained from this approach are often used as references to check the results from other methods (e.g., Stohl et al., 2003; Š;kerlak et al., 2014). This is partly because the net fluxes across the tropopause derived using the budget approach are not sensitive to the details of resolved near-tropopause phenomena, especially on seasonal or longer timescales (Holton et al., 1995; Yang et al., 2016).

Wang and Fu (2021) estimated air mass and ozone STEs based on ERA5, MERRA2, and observations using the lowermost stratosphere mass budget approach (Appenzeller et al., 1996; Schoeberl, 2004). They found that the tropical upward ozone flux, which was not considered in previous studies (e.g., Gettelman et al., 1997; Olsen et al., 2004; Yang et al., 2016), compensates for about one-third of the extratropical downward ozone fluxes and should not be neglected. In the budget approach, the 380 K isentropic surface is often used as the upper boundary of the lowermost stratosphere (e.g., Appenzeller et al., 1996; Olsen et al., 2004; Schoeberl, 2004; Wang & Fu, 2021; Yang et al., 2016). The upper boundary of the lowermost stratosphere, however, is expected to change with the changing tropical tropopause. Wang et al. (2022) proposed the dynamic upper isentrope method, in which a dynamic isentropic surface is determined by fitting to the tropical tropopause as the upper boundary of the lowermost stratosphere. Wang et al. (2022) used this method to investigate air mass and ozone STE changes in the Last Glacial Maximum as compared to the preindustrial simulations (Fu et al., 2020a, 2020b; Wang et al., 2020). Wang and Fu (2023) recently examined the STE changes from 1960 to 2099 based on multiple model simulations from Chemistry Climate Model Initiative (CCMI), showing that global ozone STE trends are -2.7% decade^{-1} for 1960–2000%, and 4.7% decade^{-1} for 2000–2099 in RCP6.0 scenario. The dynamic upper isentrope method is particularly suitable for estimating air mass and ozone STEs across different climates.

This study examines air mass and ozone STEs based on ERA5 and MERRA2, two state-of-the-art and widely used reanalyses, from 1980 to 2022. Different from Wang and Fu (2021) who used the 380 K isentropic surface as the upper boundary of the lowermost stratosphere, we employ the dynamic upper isentrope method (Wang & Fu, 2023; Wang et al., 2022) here. We also investigate the seasonal cycle and monthly anomalies of air mass and ozone STEs in ERA5 and MERRA2 in this study, in addition to the annual-mean STE climatology as in Wang and Fu (2021). This is partly motivated by the timing of ozone STEs could impact the potential mixing of stratospheric ozone into the surface because of the relatively long photochemical tropospheric ozone lifetime in winter and spring as compared to summer (Roelofs & Lelieveld, 1997). We further systematically document the main factors responsible for the discrepancies in STEs between ERA5 and MERRA2. For example, we find that differences between ERA5 and MERRA2 in the seasonal breathing of lowermost stratosphere air and ozone mass play a vital role in explaining the differences in their air mass and ozone STE seasonal cycle.

Under greenhouse gas-induced climate change, the chemistry-climate models predict an acceleration of the Brewer-Dobson circulation (BDC) (e.g., Abalos et al., 2021; Butchart, 2014; Butchart et al., 2006; Fu et al., 2015, 2019; Li et al., 2008; Lin & Fu, 2013), and increased ozone STEs (e.g., Abalos et al., 2020; Collins et al., 2003; Hegglin & Shepherd, 2009; Hess et al., 2015; Meul et al., 2018; Wang & Fu, 2023). Previous studies have also shown that the ozone STEs can be modulated by the El Niño–Southern Oscillation (ENSO), quasi-biennial oscillation (QBO), solar cycle, and volcanic eruptions (e.g., Albers et al., 2018; Hsu & Prather, 2009; Lu et al., 2017; Tie & Hess, 1997; Zeng & Pyle, 2005). Based on a chemistry-climate model using prescribed sea surface temperatures from 1990 to 2001, Zeng and Pyle (2005) showed that there was a close relationship between ENSO (with a 6-month lead) and ozone STE, with a correlation coefficient of −0.6. Using a chemistry transport model and a 5-year (2001–2005) ECMWF meteorology data, Hsu and Prather (2009) showed that 20% and 45% of the interannual ozone STE variance can be explained by the QBO in the Northern hemisphere

(NH) and Southern hemisphere (SH), respectively. However, they found that including the ENSO index does not decrease the unexplained interannual variances although the 2002–2003 El Nino is readily apparent in their ECMWF meteorological fields. With a Chemistry-Transport Model driven by two distinct European Centre forecast fields, Hsu and Prather (2014) showed that use of the BDC residual vertical velocity as a scaled proxy for ozone flux fails to capture the ozone STE interannual variability. In this study, we show that the correlation coefficient between ERA5 and MERRA2 global ozone mass STE monthly anomalies is 0.57. In other words, ERA5 and MERRA2 can only explain each other's global ozone STE monthly anomaly variance by 33%, indicating large uncertainties in STE monthly anomalies derived from ERA5 and MERRA2. We perform a multiple linear regression (MLR) analysis to investigate the interannual variabilities in air mass and ozone STEs due to ENSO, QBO, BDC, solar cycle, and volcanic aerosols. We find that the BDC can only explain a very small amount of variances (less than 5%) in the ERA5 and MERRA2 air mass and ozone STE monthly anomalies. The impacts of stratospheric volcanic aerosols on both air mass and ozone STE variabilities based on ERA5 and MERRA2 are inconclusive.

This study consists of six sections. Section 2 describes the data and method used. Section 3 presents air mass and ozone STEs from ERA5 and MERRA2, including the annual-mean climatology, seasonal cycle, and monthly anomaly. The causes for the differences between ERA5 and MERRA2 are examined in Section 4. Section 5 investigates air mass and ozone STE interannual variability associated with large-scale circulations, volcanic eruptions, and solar activities. The conclusion and discussion are given in Section 6.

2. Data and Method

We use the monthly ERA5 (Hersbach et al., 2020) and MERRA2 (Gelaro et al., 2017) reanalysis data with a 1.5° latitude by 1.5° longitude resolution to derive STEs from 01/1980 to 12/2022. The variables provided by the reanalysis, including radiative heating rate (R), temperature (T), pressure (p), ozone mass mixing ratio (q_{O_3}), are used in this study. Here the radiative heating rate is the summation of longwave and shortwave radiative heating rates.

For examining the impact of ENSO on the derived STE monthly anomalies, multivariate ENSO Index (Wolter & Timlin, 2011; https://psl.noaa.gov/enso/mei/) is used. Following Zeng and Pyle (2005), we use a 6-month lead for the ENSO index. Following Sweeney et al. (2023), the QBO index is based on ERA5 and MERRA2 monthly anomalies of zonal wind averaged over 5°S–5°N at 50 hPa with a three-month lead to obtain the maximum correlation between the STE monthly anomalies and the QBO index. The three-month lead accounts for the QBO descent from 50 hPa to the tropical tropopause (Sweeney et al., 2023). Similar results are obtained using the 50 hPa QBO index with a two-month lead. Following Lin et al. (2009), Ueyama and Wallace (2010), Fu et al. (2010), and Li and Thompson (2013), the BDC index is the three-month mean of the given month and two previous month eddy heat fluxes averaged from 10 to 50 hPa over latitudes from 25° to 90° for both hemispheres, which measures the upward propagating wave activity. The BDC time series are derived from six-hourly ERA5 and MERRA2 data (various BDC indexes including the consideration of the BDC shallow branch i.e., not part of the eddy heat flux-based BDC index are examined, and similar results are obtained; see the details in Section 5). The 10.7 cm radio flux (Tapping & Morton, 2013; https://www.ngdc.noaa.gov/stp/space-weather/solar-data/solar-features/solar-radio/noontime-flux/penticton/penticton_adjusted/tables/table_drao_noontime-flux-adjusted_monthly.txt) is used for solar activity index (Seidel et al., 2016). The stratospheric aerosol optical depth (AOD) from Sato et al. (1993; https://data.giss.nasa.gov/modelforce/strataer/) is used for the volcanic stratospheric aerosol index. Note that the stratospheric AOD was only available through September 2012, and we use the low 2012 values through 2022. We used the original AOD and solar cycle time series, but the monthly anomalies of ENSO, QBO, and BDC indexes (see Figure 13).

We use the lowermost stratosphere mass budget approach with a dynamic upper isentropic boundary (Figure S1 in Supporting Information S1) to derive STEs, which is briefly described here. More details are referred to Wang et al. (2022) and Wang and Fu (2023). Contrary to a constant 380 K isentrope (e.g., Appenzeller et al., 1996; Olsen et al., 2004; Schoeberl, 2004; Wang & Fu, 2021; Yang et al., 2016), the dynamic upper isentrope of the lowermost stratosphere (red solid line in Figure S1 in Supporting Information S1) is determined for each month by fitting an isentrope to the lapse-rate tropopause over the tropics that is equatorward of the latitudes with zero tropopause diabatic heating. The tropical boundaries are then the latitudes with zero diabatic heating at the fitted isentrope (Figure S1 in Supporting Information S1).

The diabatic flux across fitted upper isentrope, F_{upper}, over the NH extratropics, SH extratropics, and tropics is

$$F_{\text{upper}} = \iint Q\sigma \, dA, \tag{1}$$

where Q is the diabatic heating rate, $\sigma = -g^{-1}\frac{\partial p}{\partial \theta}$ is isentropic density, θ is the potential temperature, p is pressure, g is the gravitational acceleration constant, and A is the area at the fitted isentropic surface in the NH extratropics, SH extratropics, and tropics. The diabatic heating rates is calculated from

$$Q = {}_R \frac{\theta}{T}, \tag{2}$$

where R is the radiative heating rate provided by ERA5 or MERRA2, and T is the temperature. Following Appenzeller et al. (1996), the net air mass flux across the tropopause (F_{trop}) over NH and SH extratropics can be derived from the sum of the diabatic flux across the fitted upper isentrope (F_{upper}) and the lowermost stratosphere air mass change rate ($\frac{dM}{dt}$) by,

$$F_{\text{trop}} = F_{\text{upper}} + \frac{dM}{dt}, \tag{3}$$

where M is the lowermost stratosphere air mass. In the tropics, $F_{\text{trop}} = F_{\text{upper}}$. Herein F_{upper} is positive (negative) for the upwelling (downwelling) flux, and F_{trop} is negative for the net flux entering the troposphere.

Similarly, the diabatic ozone flux at the fitted upper isentropic surface, $F^{O_3}_{\text{upper}}$, is determined by

$$F^{O_3}_{\text{upper}} = \iint Q\sigma q_{O_3} dA \tag{4}$$

where q_{O_3} is the ozone mass mixing ratio. The net ozone flux across the tropopause ($F^{O_3}_{\text{trop}}$) over NH and SH extratropics can be calculated from the diabatic ozone flux at the fitted upper isentropic surface ($F^{O_3}_{\text{upper}}$) and the rate of change of ozone mass in the lowermost stratosphere ($\frac{dM_{O_3}}{dt}$),

$$F^{O_3}_{\text{trop}} = F^{O_3}_{\text{upper}} + \frac{dM_{O_3}}{dt}, \tag{5}$$

where M_{O_3} is the lowermost stratosphere ozone mass. In the tropics, $F^{O_3}_{\text{trop}} = F^{O_3}_{\text{upper}}$. Herein we neglect the ozone net chemical source in the lowermost stratosphere (CTO3) in Equation 5. That is because ERA5 does not provide ozone chemical production and loss terms. More importantly, the magnitudes of CTO3 in the lowermost stratosphere are small (e.g., Hegglin & Shepherd, 2009), including the polar stratosphere (e.g., Wang & Fu, 2021).

The summation of the downwelling air mass is not always equal to the upwelling air mass at the fitted upper isentrope. Following Olaguer et al. (1992) and Rosenlof (1995), we adjust the diabatic heating rate at the fitted upper isentrope by subtracting/adding a constant to produce a global zero net air mass flux for each month. The annual-mean adjustment is 0.03 (0.01) K day^{-1} for ERA5 (MERRA2), in good agreement with the theoretically imbalance (~0.03 K day^{-1}) shown in Olaguer et al. (1992). The adjustment applied to the diabatic heating rates has little impact on the comparison of ERA5 and MERRA2 air mass and ozone STE interannual variabilities though the adjustment may make the magnitudes of the STE climatology become slightly larger or smaller depending on the regions (not shown). Unless otherwise indicated, "diabatic heating" is referred to as diabatic heating after adjustment. The diabatic air mass and ozone fluxes are referred to as those across the fitted upper isentrope.

In this study, the monthly anomaly is derived by removing the seasonal cycle climatology for 1980–2022. To focus on the STE interannual variability, a 1-year Lanczos low-pass filter (Duchon, 1979) is applied to all the monthly anomaly time series, unless otherwise indicated. Thus, the monthly anomaly time series in this study is presented from 01/1981 to 12/2021. The MLR analysis is for the time period from 01/1981 to 12/2021. The ENSO (QBO) time series used is then from 07/1980 to 06/2021 (10/1980 to 09/2021).

3. STE Annual-Mean Climatology, Seasonal Cycle, and Monthly Anomaly

Figure 1 shows the seasonal cycle and monthly anomaly of tropical tropopause pressure (Figures 1a and 1b), temperature (Figures 1c and 1d), and fitted isentrope (Figures 1e and 1f) in the ERA5 and MERRA2. The

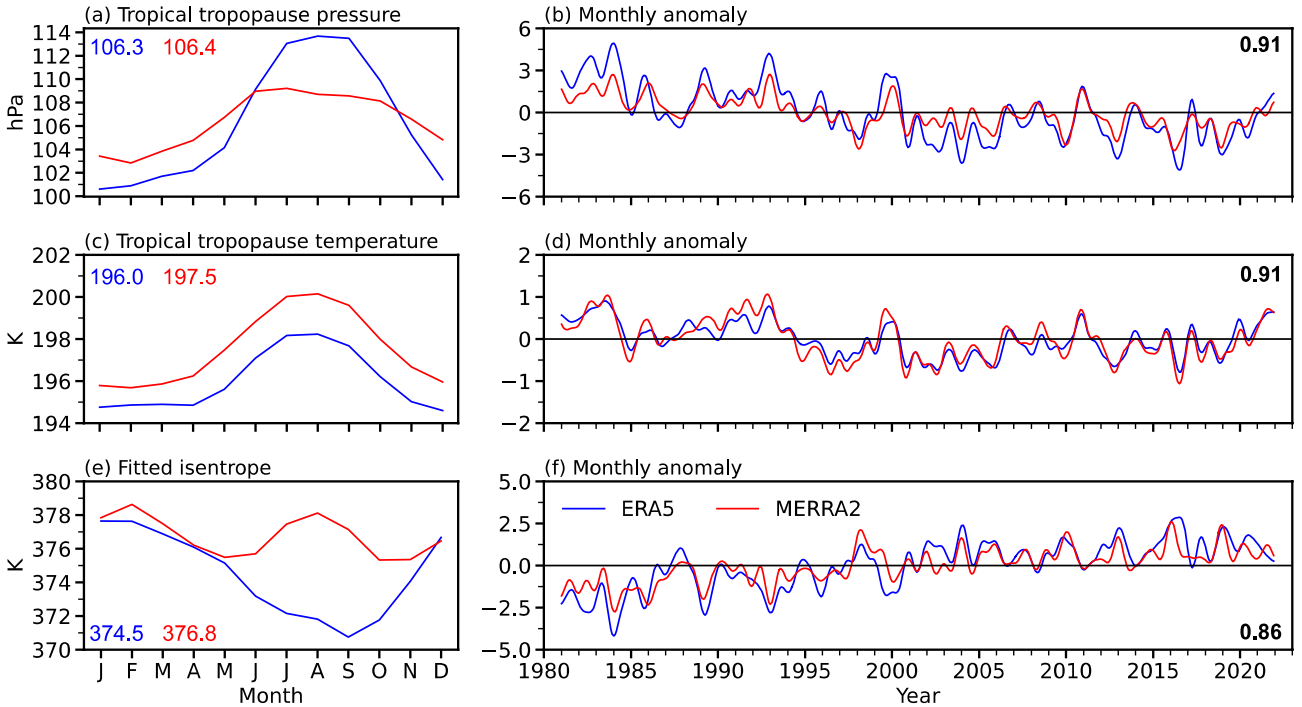

Figure 1. (a) Seasonal cycle climatology and (b) time series of monthly anomaly of the tropical-mean lapse-rate tropopause pressure (hPa) in ERA5 (blue) and MERRA2 (red) from 1980 to 2022. Panels (c) and (d), and (e) and (f) are the same as corresponding (a) and (b) but for tropical-mean lapse-rate tropopause temperature (K) and fitted isentrope (K), respectively. The numbers in (a), (c), and (e) are the corresponding annual-mean climatology values. Numbers in (b), (d), and (f) are the correlation coefficients between ERA5 and MERRA2 monthly anomalies, with bold representing statistically significant at a 95% confidence level. In Panels (b), (d), and (f), a 1-year Lanczos low-pass filter is applied to the monthly anomaly time series to focus on interannual variability and thus only the monthly anomalies from 1981 to 2021 are shown.

corresponding annual-mean values from ERA5 and MERRA2, and correlation coefficients between their monthly anomalies are provided. In ERA5, the tropical lapse-rate tropopauses have maximum pressures and temperatures from July to September, and minimum pressures and temperatures from December to February. The MERRA2 has similar seasonal patterns of tropical tropopause pressure and temperature to the ERA5. However, the tropical tropopause pressures in MERRA2 are lower than ERA5 from June to October and higher in other months, with maximum pressures around June and July, which are earlier than ERA5 (Figure 1a). The tropical tropopause temperature in MERRA2 is higher than ERA5 in all months (Figure 1c). The MERRA2 annual-mean tropical tropopause height is lower in the deep tropics but higher in the subtropics than ERA5 (not shown), leading to almost identical annual-mean tropical lapse-rate tropopause in MERRA2 (106.4 hPa) and ERA5 (106.3 hPa). However, the annual-mean tropopause temperature in MERRA2 (197.5 K) is 1.5 K higher than ERA5 (196.0 K). This is because the higher MERRA2 tropopause temperature in the deep tropics than ERA5 dominates.

The fitted isentrope is related to tropical tropopause pressure (P) and temperature (T) by $\theta = T\left(\frac{1000}{P}\right)^{0.286}$. The fitted isentrope in ERA5 has a minimum in September and a maximum in January (Figure 1e). By contrast, the fitted isentropes in MERRA2 have two peaks in February and August and two valleys in May and October. This is due to a decrease in tropopause pressure (Figure 1a) but an increase in tropopause temperature (Figure 1c) from June to August in MERRA2, leading to an increase in fitted isentrope from Jun to August (Figure 1e). On the other hand, from June to August, the ERA5 tropopause pressure increase results in a larger θ decrease than the θ increase caused by the tropopause temperature increase, leading to a decrease in fitted isentrope (Figures 1a, 1c, and 1e). Fitted isentropes in MERRA2 are larger than ERA5 almost every month, with the annual-mean value in MERRA2 (376.8 K) larger than ERA5 (374.5 K) by about 2 K (Figure 1e). This difference is primarily due to the higher tropopause temperature in MERRA2 than in ERA5 (Figure 1c). For monthly anomalies, the correlation coefficients between ERA5 and MERRA2 are 0.91, 0.91, and 0.86 for tropical tropopause pressure, temperature, and fitted isentrope, respectively. There are increasing trends in fitted isentrope from both ERA5 (0.9 K Decade^{-1}) and MERRA2 (0.6 K Decade^{-1}) (not shown), which are statistically significant at 95% confidence

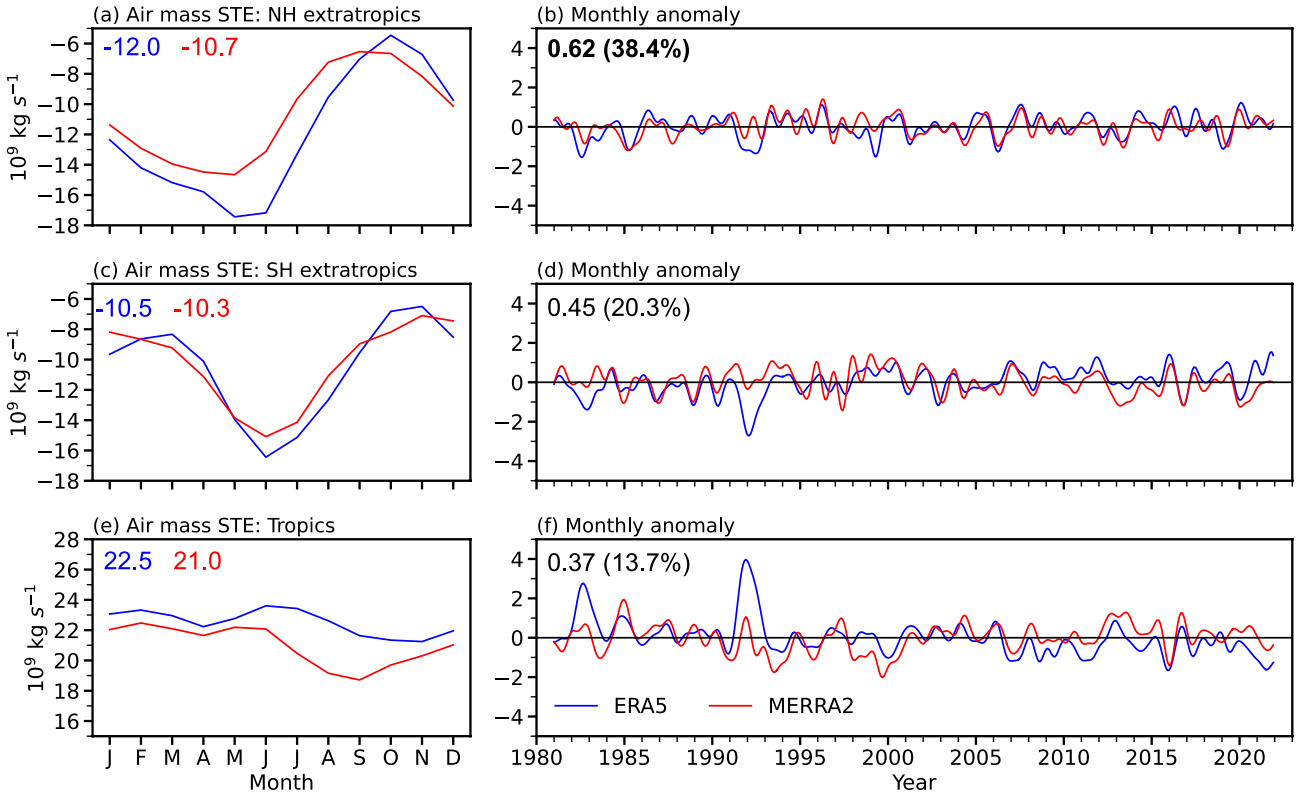

Figure 2. Same as Figure 1, but for tropopause net air mass fluxes (10^9 kg s^{-1}), that is, air mass stratosphere-troposphere exchange (STE), over (a–b) the Northern hemisphere (NH) extratropics, (c–d) Southern hemisphere (SH) extratropics, and (e–f) tropics. The numbers in the parentheses are the corresponding percentage of variances by which the ERA5 and MERRA2 air mass STE monthly anomalies can be explained by each other.

level after considering autocorrelation (Santer et al., 2000). In addition to the tropopause changes (i.e., Figures 1b and 1d), the increasing trends in fitted isentrope in ERA5 and MERRA2 could also be related to tropical warming (e.g., Woollings et al., 2023), which are coupled with the tropopause change.

The seasonal cycle and monthly anomalies of air mass STEs in the NH extratropics, SH extratropics, and tropics are shown in Figure 2, with the monthly relative anomalies shown in Figure S2 in Supporting Information S1. The seasonal cycles in air mass STEs from ERA5 and MERRA2 over all regions are similar and agree well with previous studies (e.g., Appenzeller et al., 1996; Schoeberl, 2004). The magnitudes of air mass STEs in the NH and SH extratropics have the maximum around May and June, respectively, with the minimum around October and November (Figures 2a and 2c). On the other hand, the tropical upward air mass STEs have a smaller seasonal dependence (Figure 2e). Consistent with the peak isentrope around July-September in MERRA2 (Figure 1e), the MERRA2 tropical air mass STEs in those months are smaller than in other months (Figure 2e). The annual-mean air mass STEs in the NH extratropics and tropics from ERA5 are -12 and 22.5×10^9 kg s^{-1}, respectively, the magnitudes of which are both larger than the corresponding MERRA2 values (i.e., -10.7 and 21×10^9 kg s^{-1}), while the SH extratropics annual-mean values from ERA5 (-10.5×10^9 kg s^{-1}) and MERRA2 (-10.3×10^9 kg s^{-1}) are very similar. This suggests that there is a larger difference between ERA5 and MERRA2 in the NH extratropics as compared to the SH extratropics. The annual mean climatology values of air mass STEs (Figure 2) are consistent with previous studies (e.g., Appenzeller et al., 1996; Schoeberl, 2004). Note that Appenzeller et al. (1996) used a tropical boundary of 30° N/S in their calculations (Rosenlof & Holton, 1993).

The correlation coefficients between the ERA5 and MERRA2 air mass STE monthly anomalies in the NH extratropics, SH extratropics, and tropics are 0.62, 0.45, and 0.37, respectively (Figures 2b, 2d, and 2f). Thus, the ERA5 and MERRA2 can only explain 13.7%–38.4% of each other's STE monthly anomaly variances, depending on regions. The monthly anomalies of air mass STEs range from about -15% to 15% of annual-mean climatology in the extratropics and tropics (Figure S2 in Supporting Information S1). It is interesting to note that in ERA5, there are large air mass STE anomalies (larger than 10%–20% of the annual-mean climatology) around 1983 and 1992

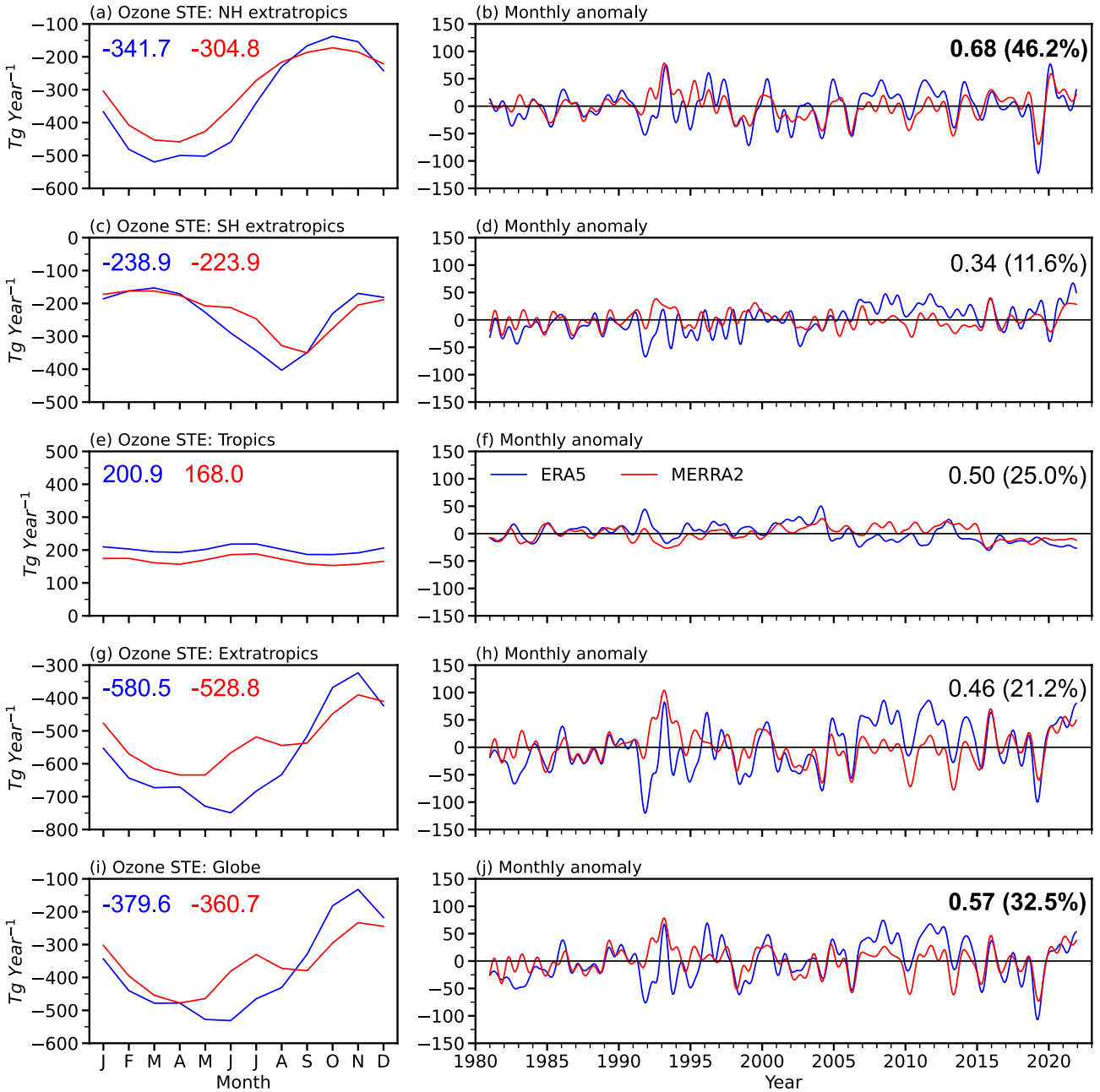

Figure 3. Same as Figure 1, but for tropopause net ozone fluxes (Tg year^{-1}), that is, ozone stratosphere-troposphere exchange (STE), over (a–b) the Northern hemisphere (NH) extratropics, (c–d) Southern hemisphere (SH) extratropics, (e–f) tropics, (g–h) extratropics, and (i–j) globe. The numbers in the parentheses are the corresponding percentage of variances by which the ERA5 and MERRA2 ozone STE monthly anomalies can be explained by each other.

in the tropics (Figure S2c in Supporting Information S1), which may be related to the El Chichon (year 1982) and Pinatubo (year 1991) volcanic eruptions (see Figure 13e and Section 5). However, the signature of these two volcanic eruptions in the MERRA2 air mass STEs is not distinct. The trends of air mass STEs over various regions for 1980–2000, 2001–2022, and 1980–2022 are shown in Table S1a in Supporting Information S1, which are either statistically insignificant or show inconsistent results from ERA5 and MERRA2.

The ozone STEs in the NH extratropics, SH extratropics, tropics, extratropics, and globe are presented in Figure 3 (see monthly relative anomalies in Figure S3 in Supporting Information S1). Consistent with previous studies (e.g., Hegglin & Shepherd, 2009; Olsen et al., 2004; Wang & Fu, 2021; Yang et al., 2016), the magnitudes of ozone STEs in the NH and SH extratropics peak around spring (Figures 3a and 3c), because of the seasonal

breathing of lowermost stratosphere ozone mass (i.e., dM_{O_3}/dt as shown in Figure 8). On the other hand, the seasonal dependence in the tropics is small (Figure 3e), due to the small seasonal dependences for air mass STE and ozone concentration in the tropics (Figures 2e and 6e). The latter is consistent with Abalos et al. (2013), who showed much smaller tracer variability on the seasonal timescale in the isentropic coordinate. The seasonal cycles of global ozone STEs closely follow those in the extratropics (Figures 3g and 3i). The annual-mean ozone STEs over the NH extratropics, SH extratropics, tropics, extratropics, and globe in ERA5 are −342, −239, 201, −581, and −380 Tg year^{-1}, respectively, with the magnitudes all larger than those of the corresponding MERRA2 values (i.e., −305, −224, 168, −529, −361 Tg year^{-1}). The magnitudes of ozone STE in the NH extratropics are larger than the SH extratropics from both ERA5 and MERRA2, agreeing with previous studies (e.g., Gettelman et al., 1997; Olsen et al., 2004; Ruiz & Prather, 2022; Yang et al., 2016). The magnitudes of ozone STEs over the extratropics derived from EAR5 (581 Tg year^{-1}) and MERRA2 (529 Tg year^{-1}) are in the range of 400–600 Tg year^{-1} from previous studies (e.g., Gettleman et al., 1997; Hsu et al., 2005; Murphy & Fahey, 1994; Olsen et al., 2001, 2004, 2013; Ruiz & Prather, 2022; Yang et al., 2016). In ERA5, the tropical ozone STE anomalies around 1983 and 1992 are not as distinguishable as the air mass STE (Figure S3c vs. Figure S2c in Supporting Information S1).

The monthly relative anomalies of ozone STEs can be up to 30% of the annual-mean climatology (Figure S3 in Supporting Information S1). The correlation coefficients between the ERA5 and MERRA2 ozone flux monthly anomalies are 0.68, 0.34, 0.50, 0.46, and 0.57 in the NH extratropics, SH extratropics, tropics, extratropics, and globe, respectively (Figures 3b, 3d, 3f, 3h, and 3j). Thus only 11.6%–46.2% of the ERA5 and MERRA2 ozone STE monthly anomaly variances can be explained by each other. For example, ERA5 and MERRA2 can only explain each other's variance in global ozone STE monthly anomalies by 32.5%. The much lower correlation coefficient between ERA5 and MERRA2 ozone STE in the SH extratropics (i.e., 0.34) may be related to the ozone fields (see Figure 12b and related discussions in Section 4.1). The ozone STE trends (Table S1b in Supporting Information S1) are either statistically insignificant or show inconsistent results from ERA5 and MERRA2.

4. Attributing the Differences Between ERA5 and MERRA2

This section investigates the differences between the ERA5 and MERRA2 air mass and ozone STEs, including their seasonal cycle, annual-mean climatology, and monthly anomalies. The air mass and ozone STEs are the summations of diabatic fluxes across fitted isentrope and the change rates of the lowermost stratosphere mass (i.e., dM/dt or dM_{O_3}/dt). The diabatic fluxes are further decided by diabatic heating, isentropic density, ozone mass mixing ratio, and tropical boundaries (see Equations 1 and 4). Here we examine the differences in those individual fields between ERA5 and MERRA2 (Section 4.1) and their contributions to the STE differences (Section 4.2). Note that the differences between ERA5 and MERRA2 in diabatic heating, isentropic density, ozone, tropical boundaries, and dM/dt or dM_{O_3}/dt can be traced back to the different practices in these two reanalyses (see Fujiwara et al., 2022 for the details), which is beyond the scope of this study.

4.1. Differences in Individual Factors That Determine the STEs

The seasonal cycle and monthly anomalies of diabatic heating are shown in Figure 4. There is diabatic cooling in the extratropics (Figures 4a and 4c) and diabatic heating in the tropics (Figure 4e). The magnitudes of diabatic cooling in the NH (SH) extratropics peak around December (May), with the minimum around May (November), while there are smaller seasonal dependences in the tropics (Figures 4a, c, and 4e). Annual-mean diabatic heating in the NH (SH) extratropics are −0.55 (−0.48) K day^{-1} in ERA5, which are close to the corresponding MERRA2 values (i.e., −0.53 and −0.49 K day^{-1}). The ERA5 diabatic heating in the tropics is larger than MERRA2 in all months (Figure 4e) by about 0.1 K day^{-1}. Correlation coefficients between ERA5 and MERRA2 monthly anomalies are 0.36, 0.51, and 0.65 in the NH extratropics, SH extratropics, and tropics, respectively.

In addition to the diabatic heating, air mass and ozone STE are dependent on the isentropic density at the fitted isentrope, which is shown in Figure 5. It is interesting to note that the isentropic density in ERA5 is larger than MERRA2 every month in both NH and SH extratropics (Figures 5a and 5c), but smaller than MERRA2 in the tropics except during July-September (Figure 5e). For the isentropic density monthly anomalies, the correlation coefficients between ERA5 and MERRA2 in NH extratropics and SH extratropics are 0.72 and 0.73 (Figures 5b and 5d), respectively. But the correlation is smaller in the tropics, which is 0.55 (Figure 5f). The tropical isentropic

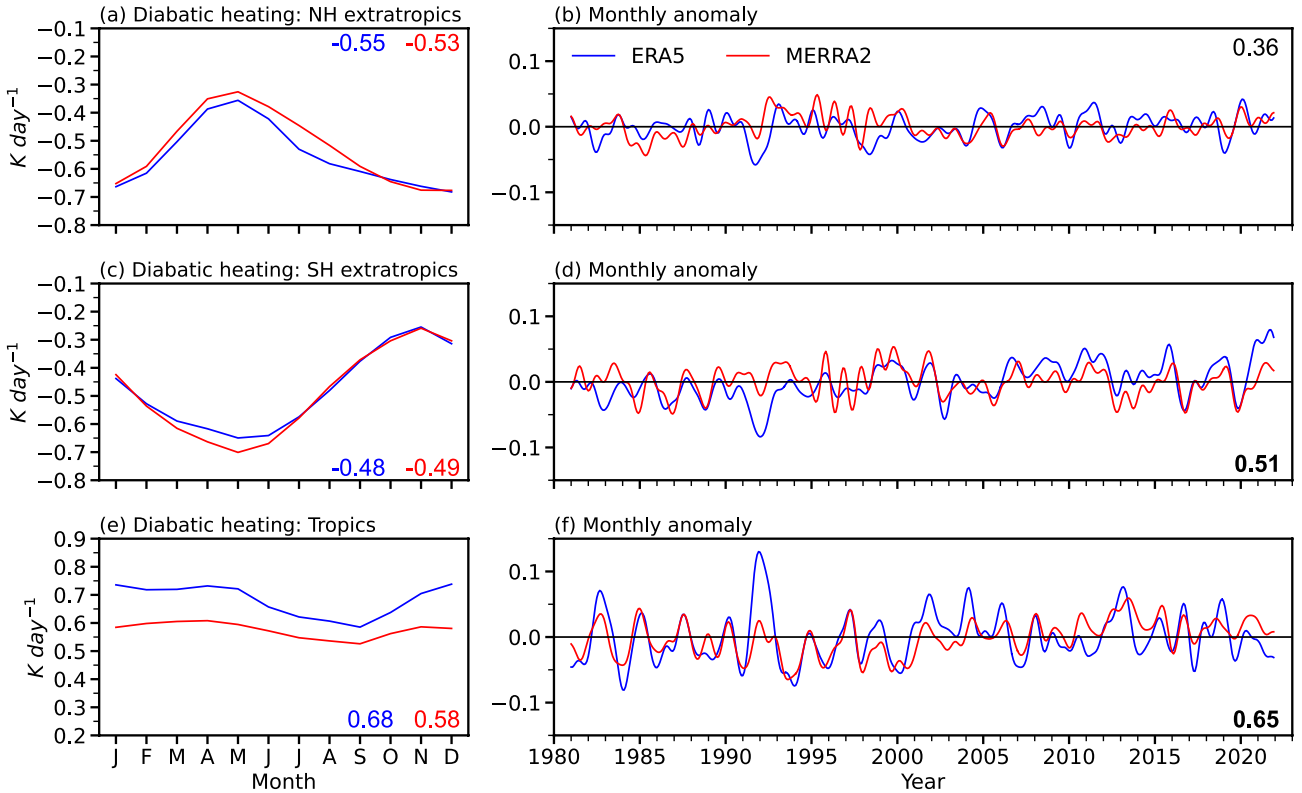

Figure 4. Same as Figure 1, but for adjusted diabatic heating (K day^{-1}) at fitted upper isentrope averaged over (a–b) the Northern hemisphere (NH) extratropics, (c–d) Southern hemisphere (SH) extratropics, and (e–f) tropics.

densities are decreasing until 2000, with no distinct trend in 2000–2022 (Figure 5f), in line with the changes in the tropical tropopause and fitted isentrope (Figure 1).

The seasonal cycle and monthly anomaly of ozone mass mixing ratios are shown in Figure 6. There is an excellent agreement in seasonal cycles and annual-mean climatology between ERA5 and MERRA2 over all regions. The ozone concentrations in the NH (SH) extratropics peak around February (August) and have the minimum around September (February-March) (Figures 6a and 6c). The seasonal cycle of ozone concentrations is small in the tropics (Figure 6e). However, the correlation coefficients between ERA5 and MERRA2 monthly anomaly are only 0.55, 0.64, and 0.53 in the NH extratropics, SH extratropics, and tropics, respectively (Figures 6b, 6d, and 6f). Figures S4, S5, and S6 in Supporting Information S1 show the relative anomalies of ERA5 and MERRA2 diabatic heating, isentropic density, and ozone, respectively. The relative anomalies range from about −15% to 15% for diabatic heating (Figure S4 in Supporting Information S1), −5% to 5% for isentropic density (Figure S5 in Supporting Information S1), and −15% to 20% for ozone concentration (Figure S6 in Supporting Information S1).

The tropical boundaries define the regions of tropics and extratropics and thus would impact air mass and ozone STE magnitudes (see Equations 1 and 4). Figure 7 shows the tropical boundary in the NH and SH, and the tropical width. There is a good agreement between ERA5 and MERRA2 in both seasonal cycles and annual-mean values (Figures 7a, 7c, and 7e). The correlation coefficients between ERA5 and MERRA2 are 0.80, 0.61, and 0.75 for the tropical boundaries in the NH and SH, and the tropical width, respectively (Figures 7b, 7d, and 7f).

The change rates of lowermost stratosphere air and ozone masses are shown in Figure 8 (see the relative monthly anomalies in Figure S7 in Supporting Information S1). As expected, the annual mean dM/dt and dM_{O_3}/dt are nearly zero (Olsen et al., 2013; Schoeberl, 2004; Wang et al., 2022; Wang & Fu, 2021). There is a larger seasonal variation of dM/dt and dM_{O_3}/dt in the NH extratropics than the SH extratropics (Figures 8a and 8e vs. Figures 8c and 8g), which are related to the hemispheric differences in the tropopause seasonal cycles (see Figure 4 in Appenzeller et al., 1996 and their discussion). It is also interesting to note that the seasonal evolutions of dM/dt

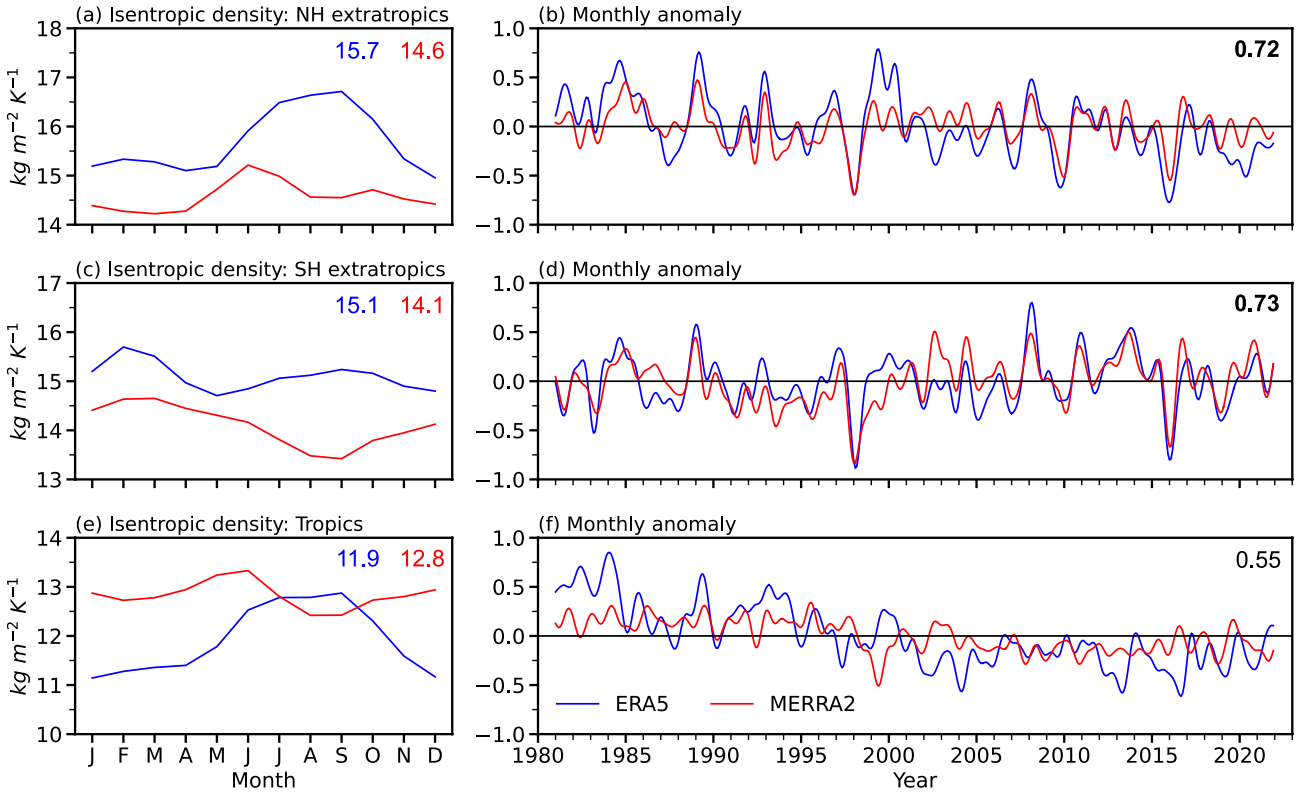

Figure 5. Same as Figure 1, but for isentropic density (kg m^{-2} K^{-1}) at fitted upper isentrope averaged over (a–b) the Northern hemisphere (NH) extratropics, (c–d) Southern hemisphere (SH) extratropics, and (e–f) tropics.

and dM_{O_3}/dt are similar in the NH extratropics, but are more different in the SH extratropics. The latter may be caused by the ozone seasonal cycle there. The correlation coefficients between ERA5 and MERRA2 dM/dt in NH and SH extratropics are 0.86 and 0.71, respectively (Figures 8b and 8d). The correlation coefficient for dM_{O_3}/dt is 0.73 in the NH extratropics and becomes much smaller in the SH extratropics (0.33) (Figures 8f and 8h). The monthly relative anomaly of dM/dt is within about ±7% of annual mean air mass STE climatology, and the relative anomaly of dM_{O_3}/dt is within about ±10% of annual mean ozone STE climatology (Figure S7 in Supporting Information S1).

4.2. Causes of the Differences in STEs Between ERA5 and MERRA2

Following Wang and Fu (2021), we quantify the STE differences in the seasonal cycle, annual-mean climatology, and monthly anomalies due to differences in diabatic heating, isentropic density, ozone, tropical boundaries, and dM/dt or dM_{O_3}/dt. For example, for ERA5 versus MERRA2 ozone STEs, the MERRA2 tropical boundaries are replaced with ERA5 tropical boundaries, retaining the MERRA2 fields of diabatic heating, isentropic density, ozone and dM_{O_3}/dt. Then we replace the MERRA2 isentropic density field with ERA5 isentropic density and retain the MERRA2 fields of diabatic heating, ozone and dM_{O_3}/dt. The MERRA2 diabatic heating field is then replaced with the ERA5 diabatic heating, with the MERRA2 ozone and dM_{O_3}/dt unchanged. Note that the downward diabatic air mass fluxes in the extratropics may not equal the upward diabatic air mass fluxes in the tropics after replacing diabatic heating or isentropic density field. Following Wang and Fu (2021), we keep adjusting the diabatic heating to keep a global zero net air mass flux at the fitted isentropic surface. We then replace the MERRA2 ozone field with the ERA5. We finally replace the MERRA2 dM_{O_3}/dt with the ERA5 field, and now all fields are from ERA5. The differences between the two calculations are referred to as STE differences due to the variable being replaced. The impacts of replacement order on the results are small (not shown).

Figure 9 shows the seasonal cycle of relative differences in air mass and ozone STEs for ERA5 versus MERRA2 due to differences in diabatic heating, isentropic density, and ozone at the fitted isentrope, tropical boundary, and

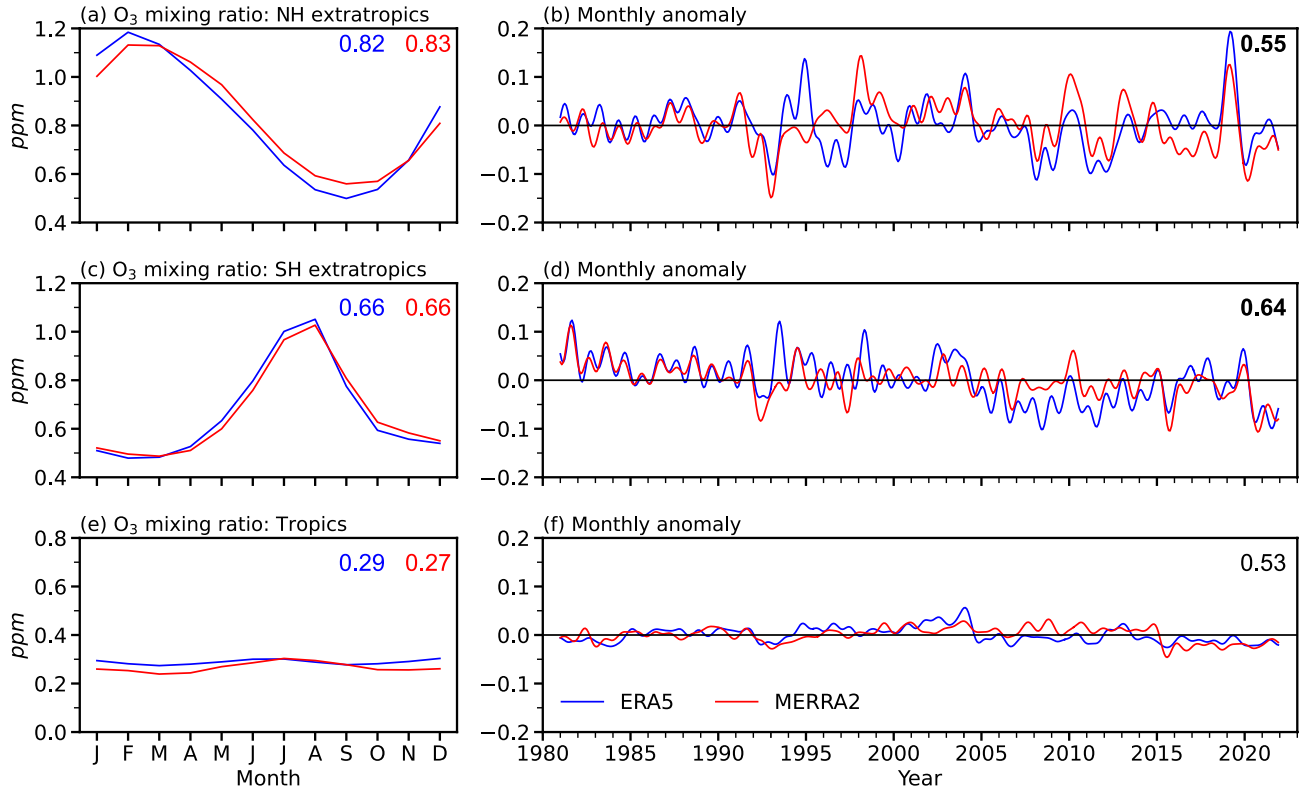

Figure 6. Same as Figure 1, but for ozone mass mixing ratio (ppm) at fitted upper isentrope averaged over (a–b) the Northern hemisphere (NH) extratropics, (c–d) Southern hemisphere (SH) extratropics, and (e–f) tropics.

seasonal breathing of lowermost stratosphere mass (i.e., dM/dt or dM_{O_3}/dt). The relative differences in air mass and ozone STEs between ERA5 and MERRA2 can be up to ±40%. Over the extratropics, the relative differences in air mass STE are generally dominated by diabatic heating and dM/dt, while isentropic density also plays a role (Figures 9a and 9c). The tropical air mass STE differences are determined by both diabatic heating and isentropic density differences. For ozone STE over the extratropics, differences are primarily due to dM_{O_3}/dt and diabatic heating generally, but ozone also plays an important role (Figures 9b, 9d, and 9g). In the tropics, the ozone STE difference is mainly due to ozone except from July to September (Figure 9f). The global ozone STE difference for ERA5 versus MERRA2, which is 40% in June and July and −40% in October and November, is largely due to the difference in dM_{O_3}/dt (Figure 9h). The differences in dM/dt between ERA5 and MERRA2 may be attributed to the tropopause permeability, which could involve the small-scale processes and vertical resolution near the upper troposphere/lower stratosphere. For dM_{O_3}/dt, the differences could also be related to the ozone concentration difference in the lowermost stratosphere.

Figure 10 presents the ERA5 versus MERRA2 relative differences in annual-mean climatology of air mass and ozone STEs. The contributions from dM/dt and dM_{O_3}/dt to the annual-mean climatology differences are zero and thus not shown in Figure 10. The relative differences in annual-mean air mass climatology, which are 12%, 2%, and 7% over NH and SH extratropics and tropics, respectively, are dominated by the differences in diabatic heating (Figure 10a). The ozone STE relative differences between ERA5 and MERRA2 are 12%, 7%, 20%, 10%, and 5% over NH and SH extratropics, tropics, extratropics, and globe, respectively. These differences in the NH and SH extratropics are dominated by diabatic heating differences. In the tropics, by contrast, the contribution from diabatic heating is comparable to but a little bit smaller than the contribution from ozone concentration difference (Figure 10b). The global ozone STE differences are primarily due to the diabatic heating differences, compensated partly by the contributions from ozone differences. Tropical boundary differences make a small contribution to air mass and ozone STE differences in all regions for both seasonal cycle and annual-mean climatology (Figures 9 and 10).

The relative differences in monthly anomalies of air mass and ozone STE between ERA5 and MERRA2 are shown in Figures 11 and 12, respectively. Here, the relative differences are the differences between ERA5 and

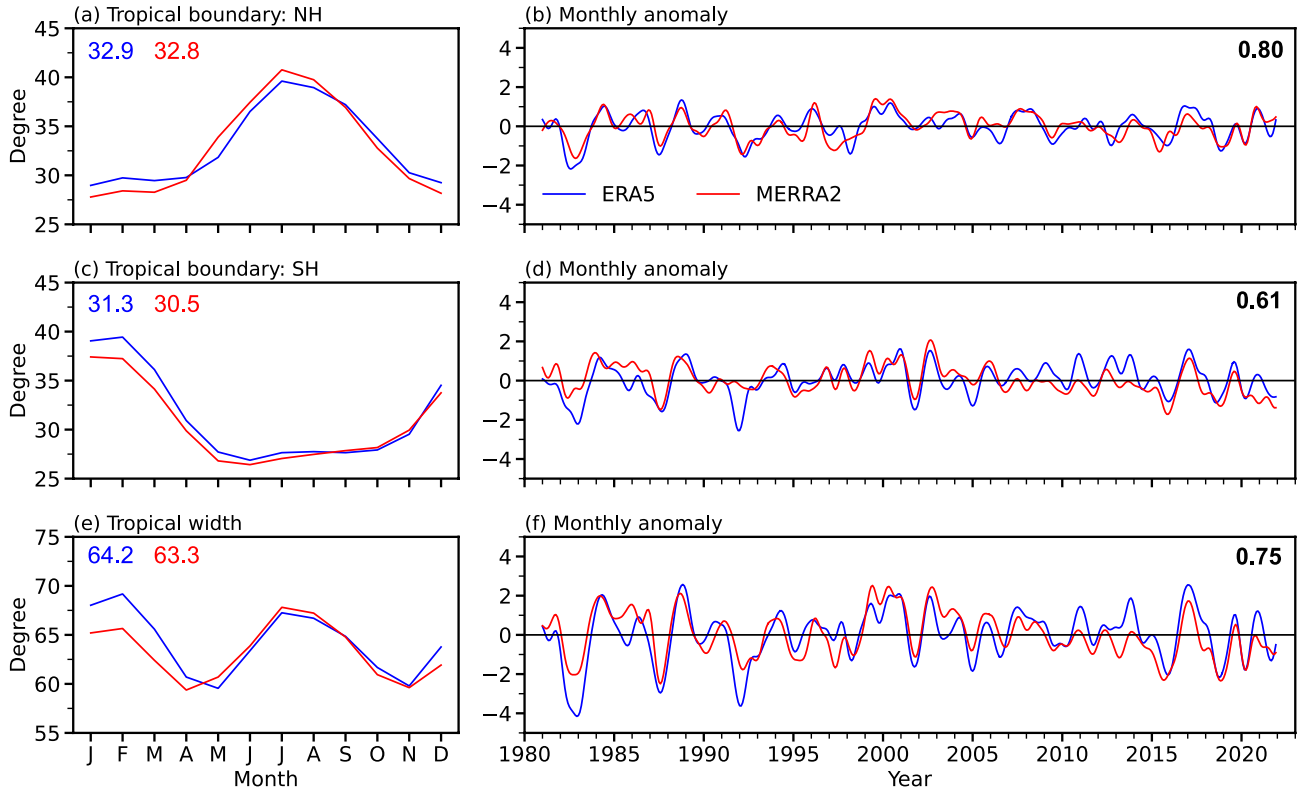

Figure 7. Same as Figure 1, but for tropical boundaries (i.e., latitudes with zero diabatic heating at the fitted upper isentrope) in the (a–b) Northern hemisphere (NH) and (c–d) Southern hemisphere (SH), and (e–f) the tropical width.

MERRA2 monthly anomalies, scaled by corresponding MERRA2 annual-mean climatology. The air mass STE differences are primarily due to diabatic heating differences in all regions, while isentropic density also plays a role (Figure 11). dM/dt also makes some contributions to the air mass STE differences over the extratropics (Figure 11). For ozone STEs over the extratropics and globe, the differences can be up to ±20%, which are dominated by the ozone in many years (Figures 12a, 12b, 12d, and 12e). Over the tropics, the ozone STE differences are mainly due to ozone differences (Figure 12c). Over all regions, the diabatic heating differences are also important, while dM_{O_3}/dt contributes to the ozone STE differences in some years. Again, the tropical boundaries play a small role in the air mass and ozone STE monthly anomaly differences (Figures 11 and 12).

5. STE Interannual Variability

Only 14%–38% (12%–46%) of the ERA5 and MERRA2 air mass (ozone) STE monthly anomaly variance can be explained by each other (Figures 2 and 3), indicating that significant non-physical signals (errors) are contained in these monthly anomalies. On the other hand, the interannual variabilities of air mass and ozone STEs can be contributed from various climate variabilities and perturbations, including ENSO, QBO, BDC, solar activities, and volcanic aerosols (e.g., Albers et al., 2018; Hsu & Prather, 2009; Lu et al., 2017; Tie & Hess, 1997; Zeng & Pyle, 2005). Here we use MLR to investigate the air mass and ozone STE interannual variabilities due to those climate variabilities and perturbations, and then examine how much variance in ERA5 and MERRA2 monthly anomalies can be explained by these interannual variability.

Figure 13 shows the predictor time series used in MLR. The heat map of the correlation coefficient matrix for those predictors is shown in Figure S8 in Supporting Information S1. The BDC and QBO indexes for ERA5 and MERRA2 are almost identical (Figures 13b and 13c), with correlation coefficients of 0.97–0.99 (Figure S8 in Supporting Information S1). ENSO, BDC, QBO, and solar cycle indices are largely independent of each other, but AOD has a relatively high correlation coefficient (0.38) with ENSO, although it is not statistically significant (Figure S8 in Supporting Information S1). In addition, the AOD signals around 1983 and 1992 in the ERA5

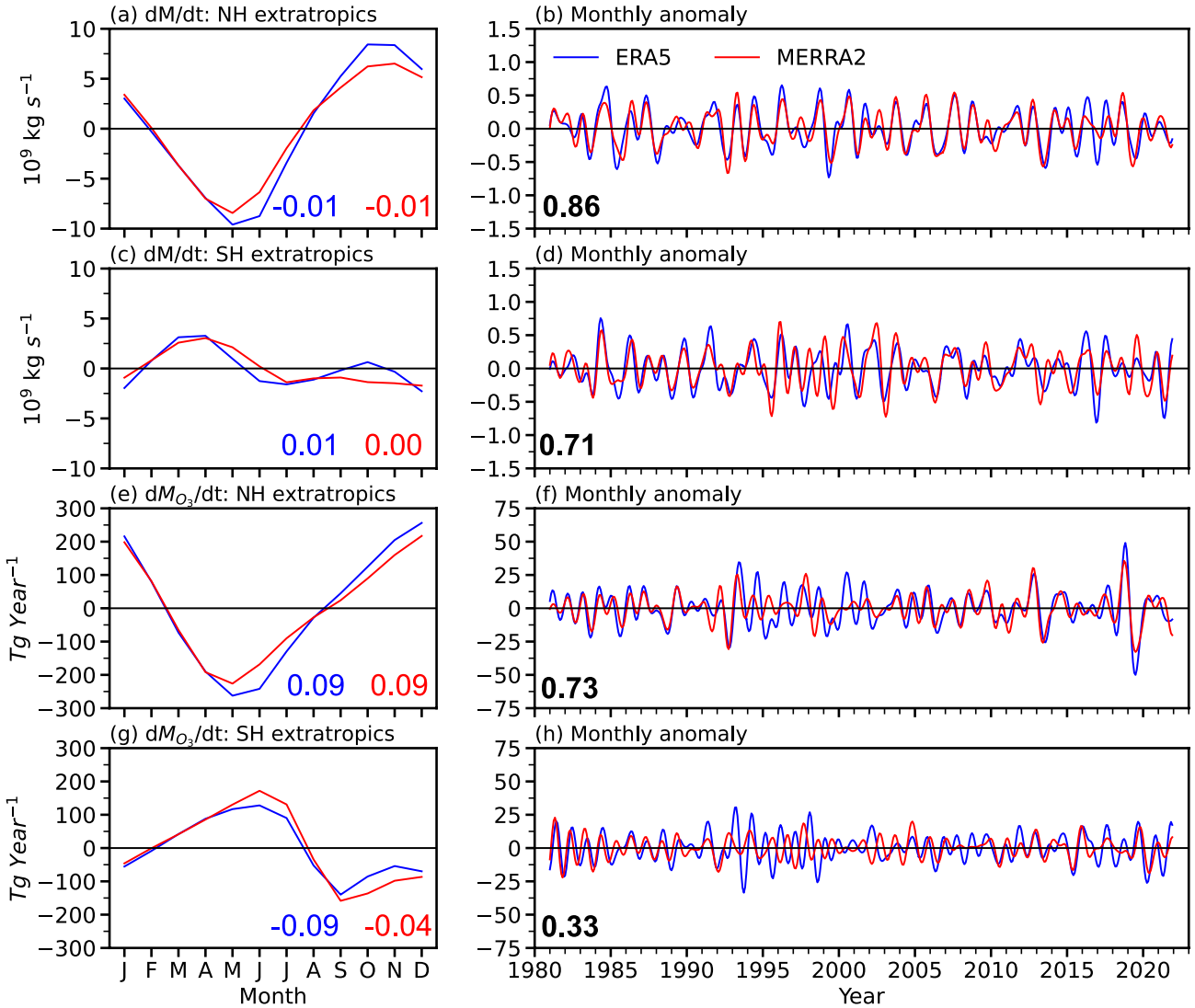

Figure 8. Same as Figure 1, but for change rates of air mass in the lowermost stratosphere (dM/dt) in the (a–b) Northern hemisphere (NH) extratropics, and (c–d) Southern hemisphere extratropics. Panels (e–f) and (g–h) are the same as corresponding (a–b) and (c–d) but for change rates of ozone mass in the lowermost stratosphere (dM_{O_3}/dt).

tropical air mass and ozone STEs are distinct (Figures 2f and 3f). Therefore, we perform MLR using the predictors of ENSO, QBO, BDC, solar, and AOD to derive the regression coefficients for these predictors. Then, the air mass and ozone STE time series due to ENSO, QBO, and BDC from 1981 to 2021 (first columns in Figures 14 and 15) are derived using these coefficients along with the ENSO, QBO, and BDC time series. We then obtain the time series due to the solar cycle (second columns in Figures 14 and 15) and AOD (third columns in Figures 14 and 15) from 1981 to 2021. The fourth columns in Figures 14 and 15 are the residual time series that cannot be explained by ENSO, QBO, BDC, solar, and AOD.

The correlation coefficients between ERA5 and MERRA2 air mass STE time series predicted by ENSO, QBO, and BDC together are 0.98, 0.61, and 0.91 over NH and SH extratropics and tropics, respectively (Figures 14a, 14e, and 14i). The correlation coefficients between ERA5 and MERRA2 ozone STE time series predicted by ENSO, QBO, and BDC together are relatively high in the NH extratropics (0.96), extratropics (0.87), and globe (0.94) (Figures 15a, 15m, and 15q), but smaller in the SH extratropics (0.64) and tropics (0.62) (Figures 15e and 15i). We can see that the variability explained by ENSO, BDC, and QBO together is much smaller than those shown in the residual (Figures 14 and 15). For air mass STE, the solar cycle contributions are in the opposite signs for ERA5 and MERRA2 in all regions (Figures 14b, 14f, and 14j). For ozone STE, the signs of

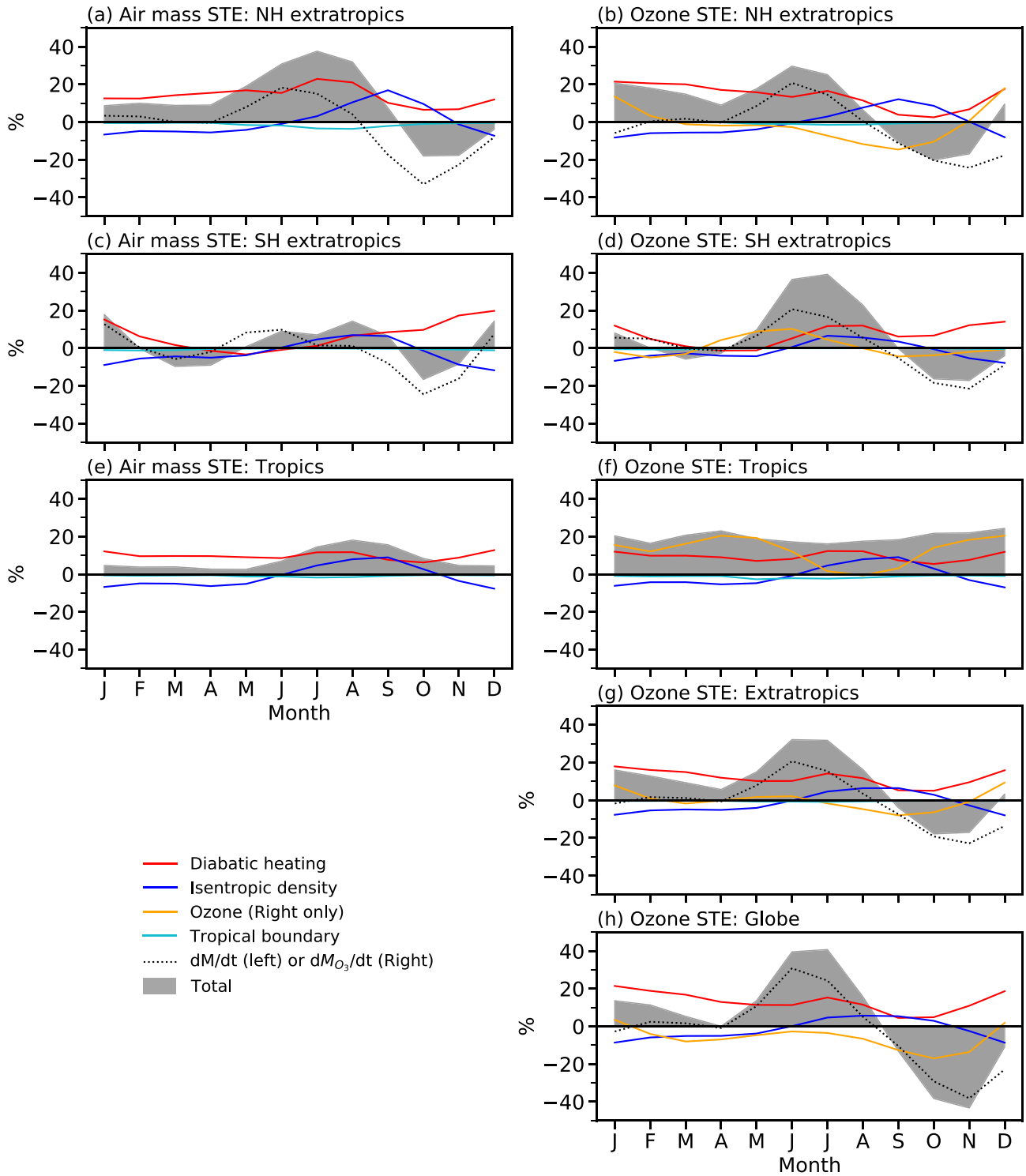

Figure 9. Relative differences between ERA5 and MERRA2 (gray shading) in seasonal cycle of air mass (left) and ozone (right) stratosphere-troposphere exchanges (STEs) over (a–b) the Northern hemisphere (NH) extratropics, (c–d) Southern hemisphere (SH) extratropics, (e–f) tropics, (g) extratropics, and (h) globe. Red, blue, and cyan lines are the air mass and ozone STE relative differences due to the differences in diabatic heating and isentropic density at the fitted isentrope, and tropical boundaries, respectively. The orange lines in the right panels are the ozone STE relative differences due to ozone mixing ratio differences. The black dotted lines are the STE relative differences due to differences in the change rates of air mass (dM/dt, left) and ozone mass (dM_{O_3}/dt, right) in the lowermost stratosphere. The relative differences are calculated by using the corresponding MERRA2 monthly climatology as the denominator.

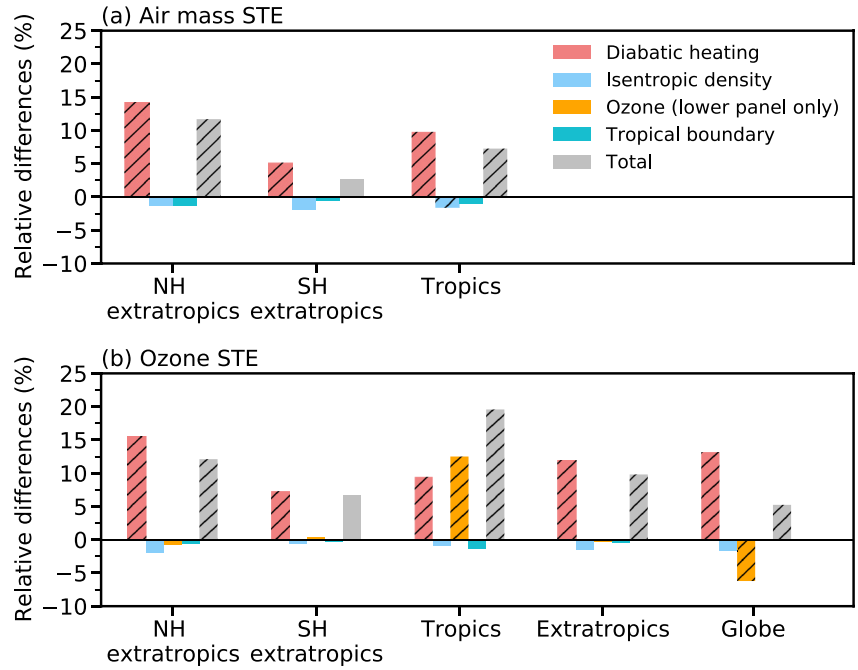

Figure 10. (a) Relative differences between ERA5 and MERRA2 (gray colors) in annual-mean air mass stratosphere-troposphere exchange (STE) climatology over the Northern hemisphere (NH) extratropics, Southern hemisphere (SH) extratropics, and tropics. Panel (b) is the same as (a) but for ozone STE relative differences in the NH extratropics, SH extratropics, tropics, extratropics, and globe. Red, blue, and cyan colors indicate the air mass and ozone STE differences due to the differences in diabatic heating and isentropic density at the fitted isentrope, and the tropical boundaries. Orange colors in (b) indicate the ozone STE differences due to ozone mass mixing ratio differences. The annual-mean climatology of change rates of air and ozone mass in the lowermost stratosphere are zero, and their effects are also zero, which are thus not shown here. The bars with the slant lines indicate the relative differences are statistically significant at a 95% confidence level.

solar cycle contributions are opposite for ERA5 and MERRA2 in the SH extratropics (Figure 15f) but the same in other regions (Figures 15b, 15j, 15n, and 15r). On the other hand, the AOD contributions are in opposite signs for ERA5 and MERRA2 in all regions for air mass and ozone STE, except for the air mass STE in the NH extratropics (Figure 14c). For air mass STEs, the AOD leads to about 10%–20% positive relative anomalies in all regions around the years 1983 and 1992 in the ERA5, while the AOD signals are close to zero in the MERRA2 (Figures 14c, 14g, and 14k), consistent with Figure 2. Thus, the impacts of volcanic stratospheric aerosols on both air mass and ozone STEs are inconclusive based on ERA5 and MERRA2 reanalyses, which may be related to how aerosol is assimilated in ERA5 and MERRA2 (Fujiwara et al., 2022). It is interesting to note that the correlation between the ERA5 and MERRA2 residual air mass STEs becomes larger over SH extratropics and tropics while it remains the same in the NH extratropics (Figure 14 vs. Figure 2). The correlation coefficients between the ERA5 and MERRA2 residual ozone STEs are also somewhat larger than those before removing the known climate variabilities and perturbations in all regions (Figure 15 vs. Figure 3). The correlation coefficients of the residual time series between ERA5 and MERRA2 do not become smaller as compared with the original time series because the AOD and solar cycle play very different (often opposite) roles in modulating the STEs in ERA5 and MERRA2.

We define the variances explained by predictors using the adjusted coefficient of determination (R^2), which accounts for artificially high R^2 due to collinearity among predictors used in MLR (Lindeman, 1980). Figure 16 shows R^2 for air mass and ozone STE explained by ENSO, BDC, QBO, solar cycle, and volcanic aerosols, along with R^2 that cannot be explained by predictors (i.e., residual). For air mass STE, the variances in all regions explained by ENSO are 0.3%–4.3% in ERA5 and MERRA2. As expected, the air mass STE variances explained by QBO are much larger in the tropics (15.6%–20.6%) than in the extratropics (3.8%–13.1%). Figure 16 also indicates that the QBO play a more important role in the NH extratropics than the SH extratropics. This is because the QBO-induced mean meridional circulation is mainly confined in the winter hemisphere, but is located more poleward in the NH during the boreal winter than that in the SH during the austral winter (see Figure 5 in Pahlavan et al., 2021). QBO signals obviously stand out in Figures 14a, 14e, and 14i.

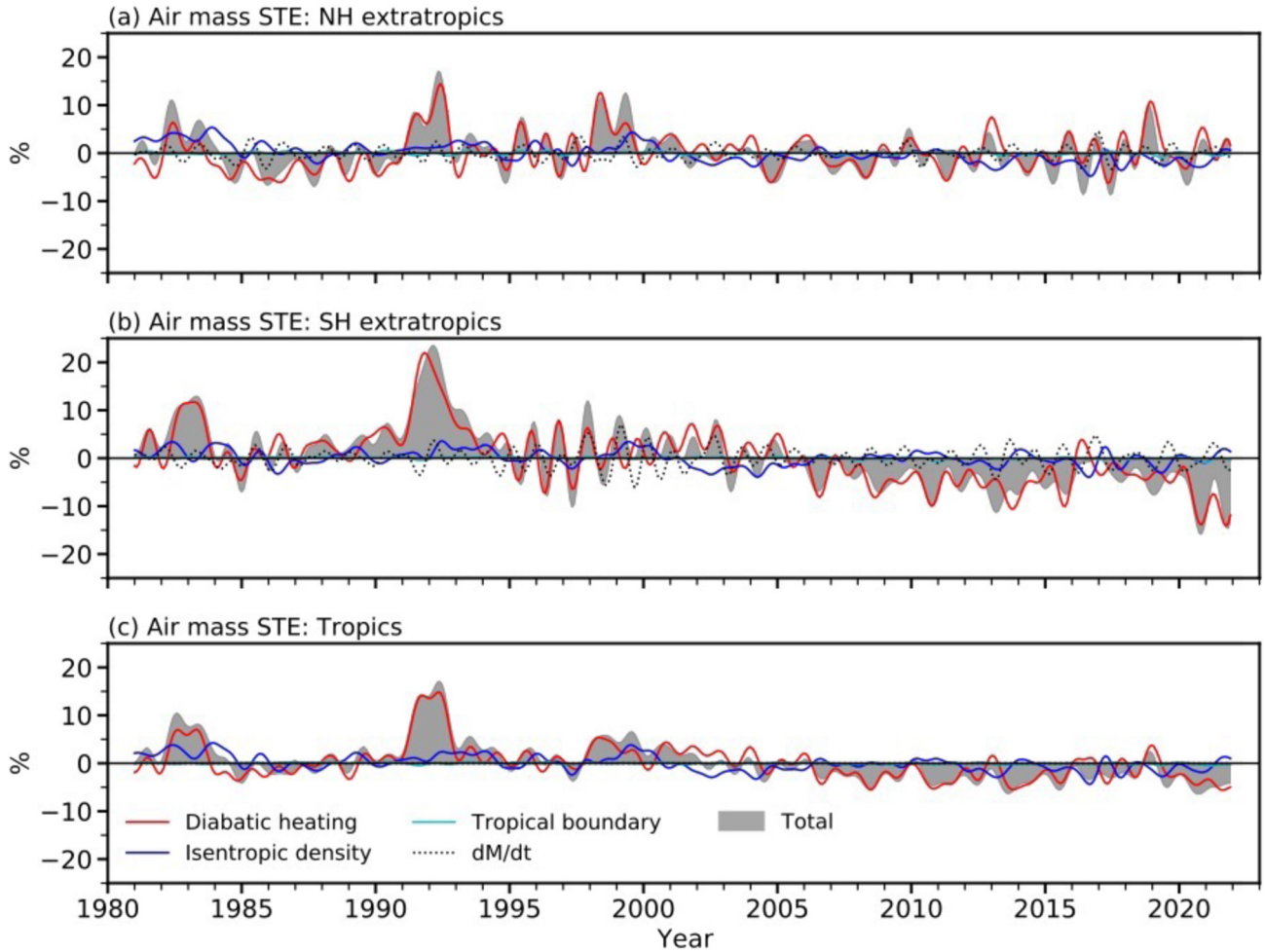

Figure 11. Relative differences between ERA5 and MERRA2 (gray shading) in monthly anomalies of air mass stratosphere-troposphere exchange (STE) over (a) the Northern hemisphere (NH) extratropics, (b) Southern hemisphere (SH) extratropics, and (c) tropics. The red, blue, and cyan solid lines are the STE relative differences due to the differences in diabatic heating and isentropic density at the fitted isentrope, and the tropical boundaries. The black dotted lines in (a) and (b) are the STE relative differences due to differences in change rates of air mass in the lowermost stratosphere (dM/dt). The corresponding MERRA2 air mass annual-mean climatology values are used as the denominator for the relative differences. In panels (a), (b), and (c), a 1-year Lanczos low-pass filter is applied to focus on interannual variability and thus only the monthly anomalies from 1981 to 2021 are shown.

Interestingly, the BDC can only explain 0.5%–1.7% of air mass STE variances in all regions in ERA5 and MERRA2. Similar results are obtained by using different BDC indexes, including the three-month mean eddy heat flux at 100 hPa over latitudes from 25° to 90° and the tropical air mass flux at 70 hPa based on residual vertical velocity (Rosenlof, 1995) (not shown). Sweeney and Fu (2023) recently showed that the BDC shallow branch that was not part of the eddy heat flux-based BDC can explain significant portion of the tropical cold point temperature interannual variability. We calculate the tropical air mass fluxes at 100 hPa based on the transformed Eulerian mean (TEM) vertical velocity (Andrews et al., 1987) by using the 6-hourly ERA5 and MERRA2 data from 1980 to 2022. It is interesting to note that the correlation coefficient between the ERA5 and MERRA2 tropical air mass flux monthly anomalies at 100 hPa is 0.63, similar to that between the ERA5 and MERRA2 diabatic heating over the tropics (Figure 4f). As shown in Figures 9–12, a large proportion of air mass and ozone STE differences between ERA5 and MERRA2 are attributed to the diabatic heating differences. Following Sweeney and Fu (2023), we use the tropical air mass flux at 100 hPa after removing QBO, ENSO, and eddy heat flux-based BDC to consider the impact of the BDC shallow branch that was not included in the eddy heat flux-based BDC. Consideration of this BDC shallow branch does not change the results: the two BDC indices together can only explain 1.6%–3.1% of the air mass STE variances.

The solar cycle can explain 0.0%–6.3% variances over extratropics and 3.0%–7.9% variances over tropics. The air mass STE variances explained by AOD are much larger for ERA5 than MERRA2, which are 16.3%, 28.8%,

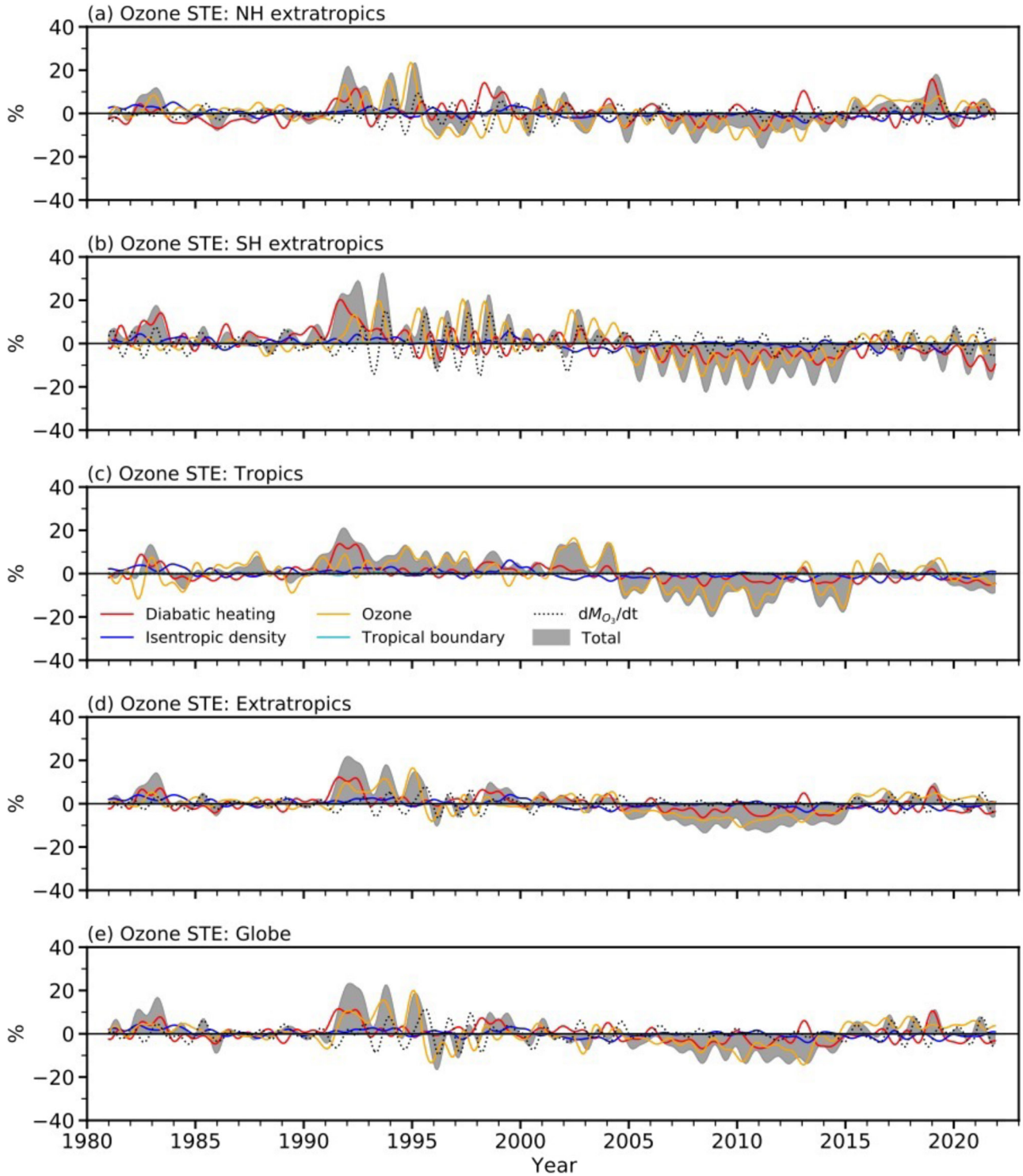

Figure 12. Same as Figure 11, but for relative differences in the monthly anomalies of ozone stratosphere-troposphere exchange (STE) over (a) the Northern hemisphere (NH) extratropics, (b) Southern hemisphere (SH) extratropics, (c) tropics, (d) extratropics, and (e) globe. Orange lines are the ozone STE relative differences due to differences in ozone mass mixing ratio. The black dotted lines in (a), (b), (d), and (e) are the ozone STE relative differences due to differences in change rates of ozone mass in the lowermost stratosphere (dM_{O_3}/dt).

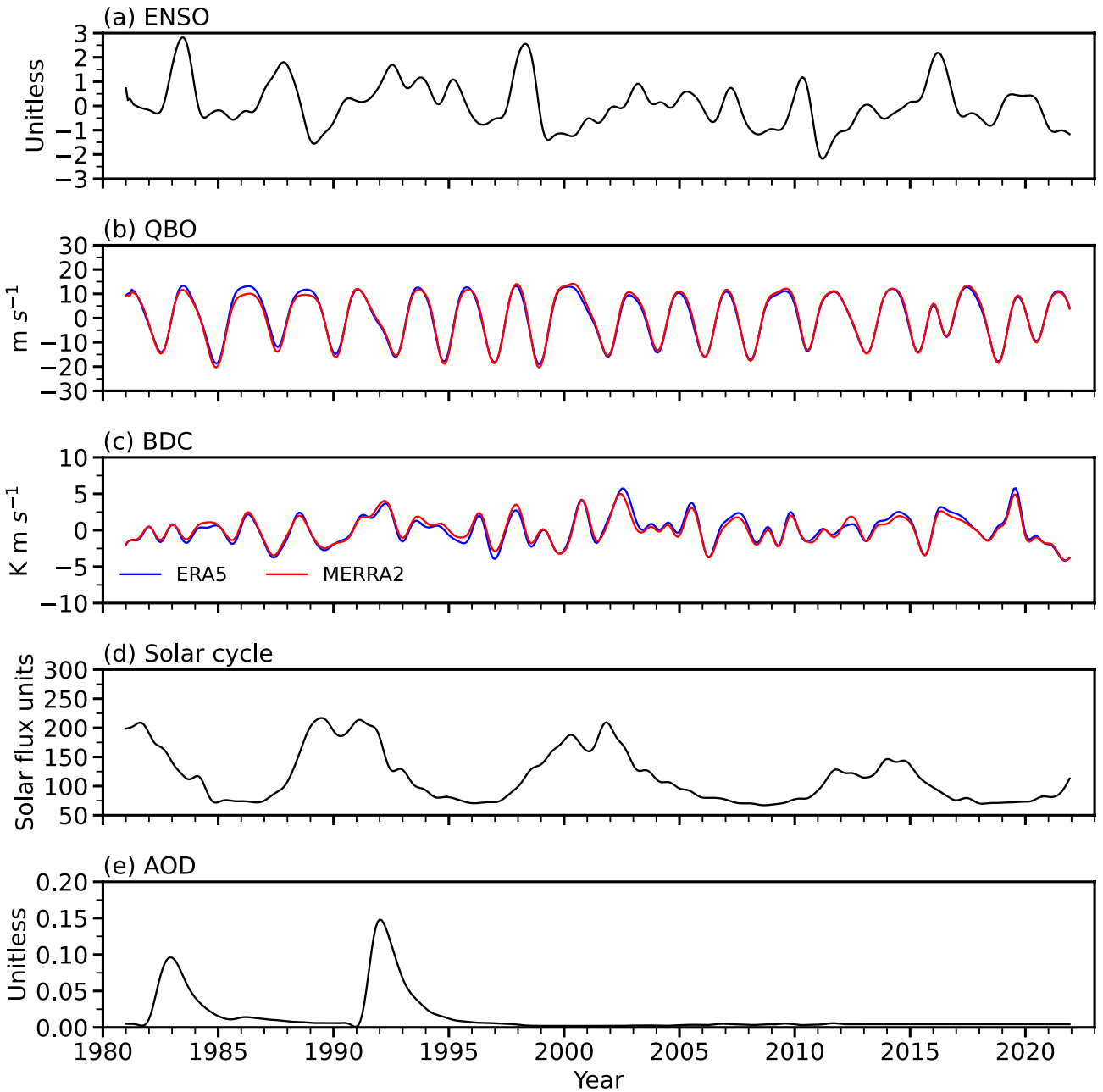

Figure 13. Predictor time series from 1981 to 2021 used in multiple linear regression analyses, including indices of (a) El Niño-Southern Oscillation (ENSO), (b) Quasi-Biennial Oscillation (QBO), and (c) Brewer-Dobson circulation (BDC), (d) solar cycle (1 solar flux unit = 10^{-22} W m^{-2} Hz^{-1}), and (e) stratospheric aerosol optical depth (AOD). The time series in (a), (d), and (e) are derived from observation. The ENSO index in (a) has a 6-month lead (i.e., from 07/1980 to 06/2021) to investigate its impact on air mass and ozone STEs from 01/1981 to 12/2021 in multiple linear regression analyses. The QBO index in (b) is the time series of monthly anomalies of zonal wind at 50 hPa averaged over 5°S–5°N with a three-month lead (i.e., from 10/1980 to 09/2021) from ERA5 (blue line) and MERRA2 (red line). In (c), the BDC time series are derived from six-hourly ERA5 and MERRA2 data. A 1-year Lanczos low-pass filter is applied to focus on interannual variability.

and 43.3% over NH and SH extratropics, and tropics, respectively, from ERA5, but are all close to zero from MERRA2, consistent with Figures 2 and 14. We see from the residuals in ERA5 (MERRA2) that 58.7%–68.5% (84.6%–85.7%) of variances cannot be explained over extratropics, while 28.1% (71.7%) variances cannot be explained over tropics. The difference between ERA5 and MERRA2 is mainly associated with the impact of AOD, which again may be related to how aerosol is assimilated in ERA5 and MERRA2 (see Fujiwara et al., 2022).

For ozone STEs over the extratropics and globe, the variances in ERA5 and MERRA2 monthly anomalies explained by ENSO are 5.0%–17.3% in the ERA5, which are all larger than the MERRA2 (0.1%–5.0%)

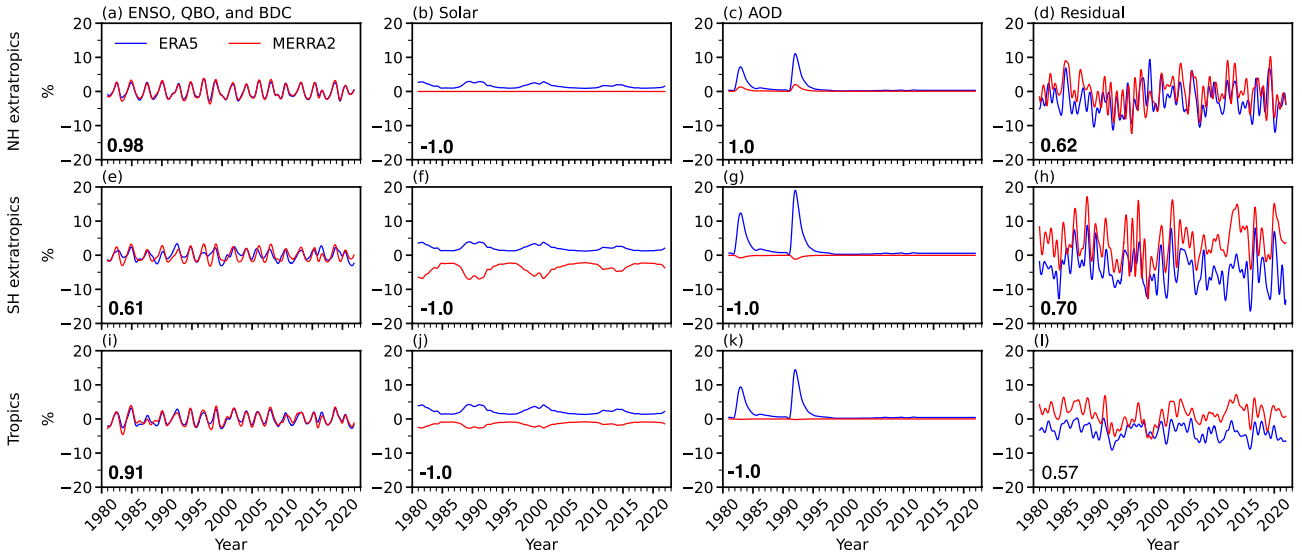

Figure 14. Monthly anomaly of air mass stratosphere-troposphere exchange (STE) scaled by the corresponding annual-mean climatology STEs in the ERA5 (blue) and MERRA2) (red) from 1981 to 2021 due to (a) the combination of El Niño-Southern Oscillation (ENSO), Quasi-Biennial Oscillation (QBO), and Brewer-Dobson circulation (BDC), (b) solar cycle, (c) Stratospheric aerosol optical depth (AOD), and (d) the residual that cannot be explained by ENSO, QBO, BDC, solar, and AOD in the Northern hemisphere (NH) extratropics. Panels (e–h) and (i–l) are the same as (a–d) but for the Southern hemisphere (SH) extratropics and tropics, respectively. The values shown within panels are the correlation coefficients between ERA5 and MERRA2 monthly anomalies, with bold representing statistically significant at a 95% confidence level.

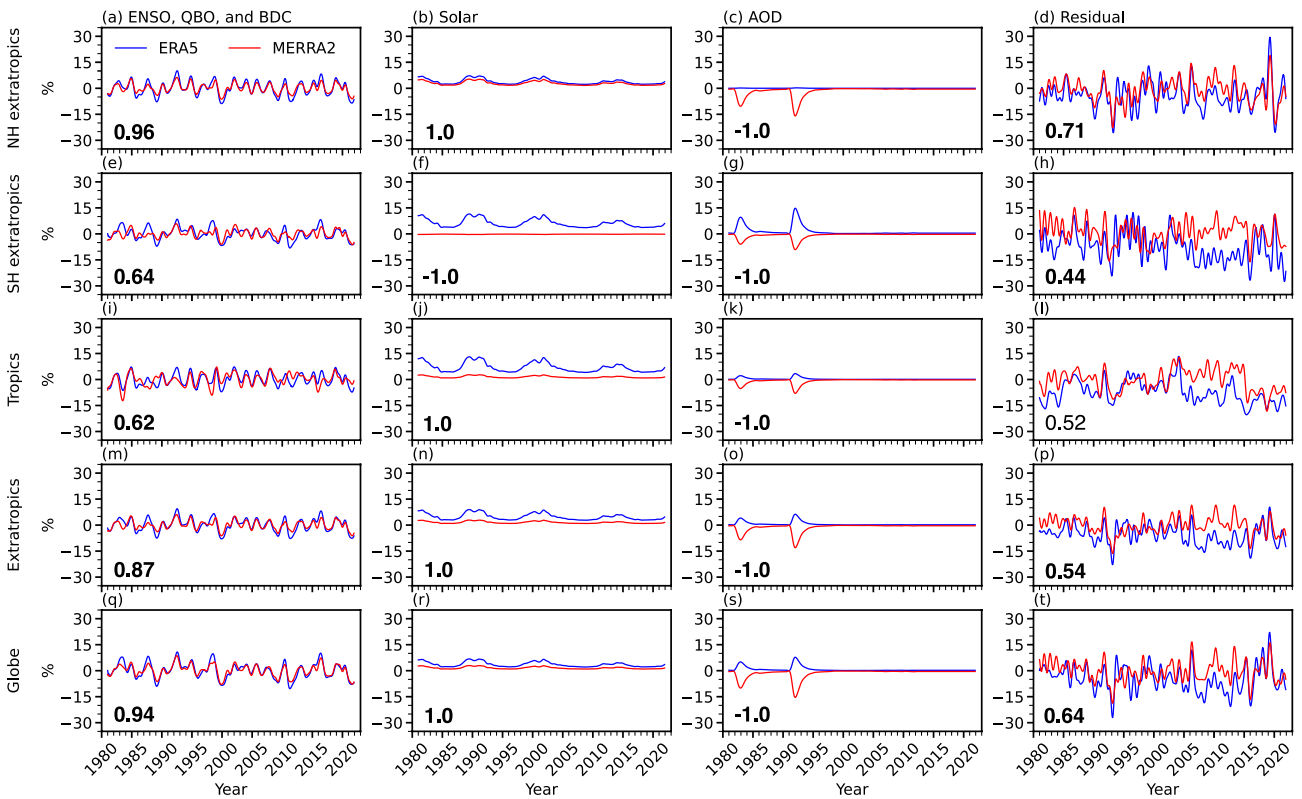

Figure 15. Same as Figure 14, but for monthly relative anomaly of ozone stratosphere-troposphere exchange (STE) over (a–d) the Northern hemisphere (NH) extratropics, (e–h) Southern hemisphere (SH) extratropics, (i–l) tropics, (m–p) extratropics, and (q–t) globe.

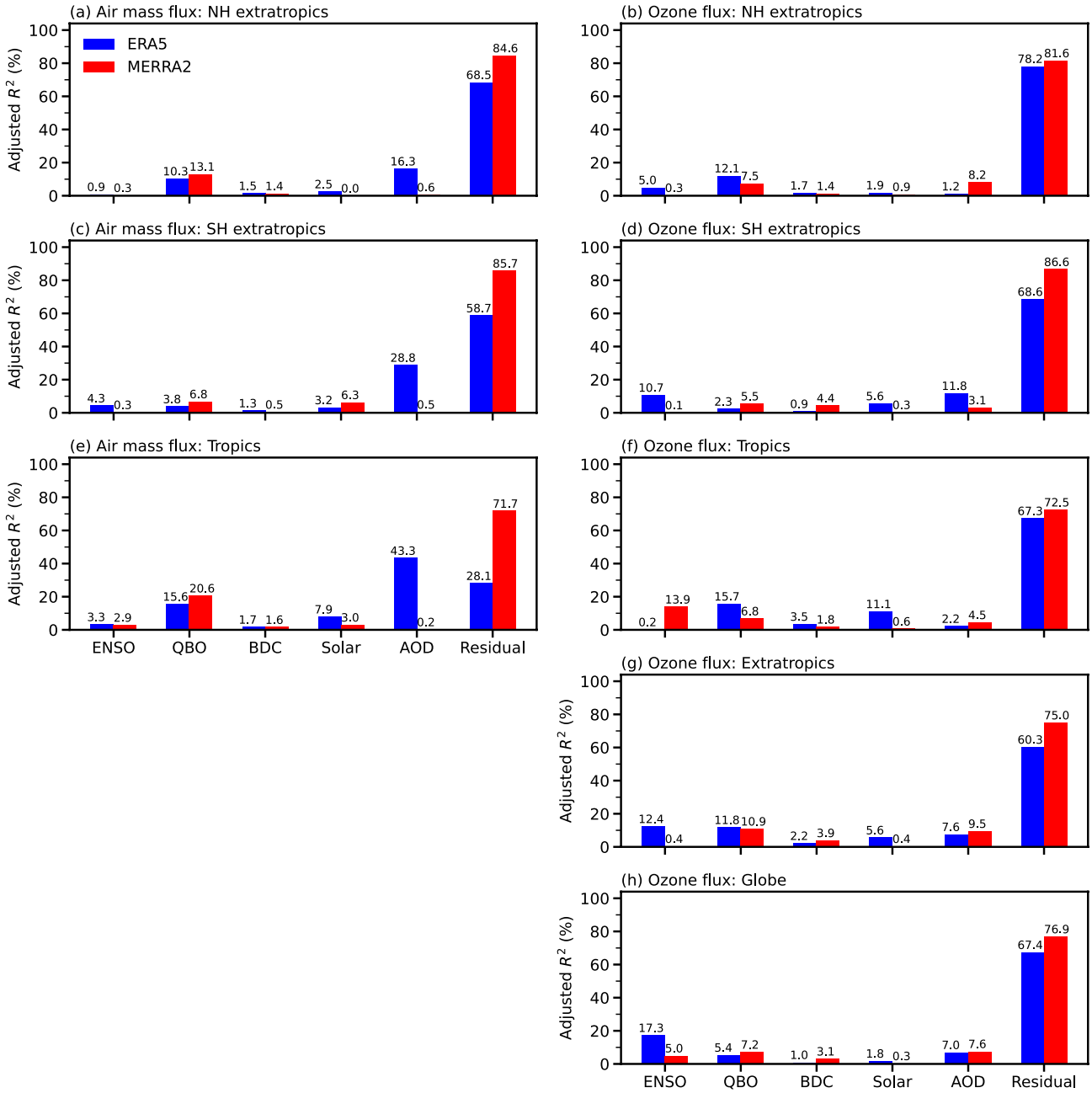

Figure 16. The adjusted relative variance (i.e., R^2) explained by each predictor and the residual for ERA5 (blue) and MERRA2 (red) air mass stratosphere-troposphere exchange (STE) in (a) the Northern hemisphere (NH) extratropics, (c) Southern hemisphere (SH) extratropics, and (e) tropics. (b), (d), (f), (g), and (h) are the same as (a) but for ozone STE in the NH extratropics, SH extratropics, tropics, extratropics, and globe, respectively. Values shown at the top of color bars are the corresponding adjusted R^2.

(Figures 16b, 16d, 16g, and 16h). Over the tropics, by contrast, the ENSO explained variance in the ERA5 (0.2%) is smaller than the MERRA2 (13.9%). Depending on the regions and reanalysis, the variances explained by QBO are larger or smaller than ENSO, which are 2.3%–15.7% for ERA5 and 5.5%–10.9% for MERRA2. The BDC can only explain 0.9%–4.4% of ozone STE variance, while solar activities can explain 0.3%–11.1% of the variance. Contrary to air mass STE, the variances that AOD can explain are similar for ERA5 (1.2%–11.8%) and MERRA2 (3.1%–9.5%). The residual variances are 60.3%–78.2% for ERA5 and 72.5%–86.6% for MERRA2. For the global ozone STE monthly anomalies, ENSO, QBO, BDC, solar cycle, and volcanic aerosols can explain the variance by 5.0%–17.3%, 5.4%–7.2%, 1.0%–3.1%, 0.3%–1.8%, 7.0%–7.6%, respectively, with a residual variance as large

as 67.4%–76.9% (Figure 16h). We also examine the air mass and ozone diabatic fluxes using the fixed upper isentrope at 380K and performed the MLR, and the results remain quite similar (not shown). Furthermore, the BDC by considering both eddy heat flux-based index and the BDC shallow branch index can explain the ozone STE variance less than 4.5% over all regions from both reanalyses (the only exception is from ERA5 over the tropics where the explained variance increases from 3.5% to 8% by using both indices vs. using eddy heat flux-based BDC index only).

Based on three reanalyses (ERA-Interim, MERRA, and JRA-55), Abalos et al. (2015) showed that for the period 1970–2012 the variances of tropical upwelling at 100 hPa can be explained by the QBO and ENSO by about 0%–7.5% and 0%–12%, respectively, depending on the reanalysis and methods used to estimate the tropical upwelling (see their Figure 9). Our results for the small variances of air mass STEs explained by the QBO and ENSO are generally consistent with Abalos et al. (2015). For the period of 1990–2002 considered in Zeng and Pyle (2005), we get a correlation coefficient of −0.52 between the ENSO index with a 6-month lead and the global ozone STE from the ERA5, which is somewhat smaller than the correlation coefficient of −0.6 from Zeng and Pyle (2005). However, the correlation coefficient is only −0.07 in the MERRA2. In our study, the QBO impact on air mass and ozone STEs can be clearly seen in the first column of Figures 14 and 15, and it can explain 3.8%–20.6% of air mass STE variances and 2.3%–15.7% of ozone STE variances. The latter is smaller than the QBO contribution (20%–45%) shown in Hsu and Prather (2009). Such a discrepancy may be related to the different data used (reanalysis vs. meteorology data), and different period considered (1981–2021 vs. 2001–2005). It may also be related to the method used, that is, the ozone STEs in this study are integrated over the NH extratropics, SH extratropics and tropics (which may average out part of QBO signal), while in Hsu and Prather (2009) the QBO impact was quantified with latitudinal distribution (see their Figure 6).

Finally, it is worth pointing out that as expected, the easterly QBO enhances the air mass and ozone STEs in both ERA5 and MERRA2 over all regions based on our analyses (not shown), which can also be seen by comparing Figures 14 and 15 with Figure 13. The El Nino phase of the ENSO enhances the air mass and ozone STEs in ERA5 while ENSO shows little impact in MERRA2 except over tropics where the El Nino decreases the ozone STE (not shown). The solar activity enhances the ozone STEs in ERA5 but show little impact in MERRA2 (Figure 15). That the solar activity enhances the ozone STEs in ERA5 is consistent with an increased ozone concentration in response to an increase in the Sun's UV radiation output (e.g., WMO, 2010).

6. Conclusion and Discussions

This study investigates the air mass and ozone STEs in ERA5 and MERRA2 from 1980 to 2022 using the dynamic upper isentrope method where the upper isentrope of the lowermost stratosphere is determined by fitting to the tropical lapse-rate tropopause instead of using a fixed isentrope of 380 K. The annual-mean climatology, seasonal cycle, and monthly anomalies of air mass and ozone STEs from ERA5 and MERRA2 are derived, and the differences between ERA5 and MERRA2 are systematically examined. We further investigate the interannual variability of air mass and ozone STEs associated with ENSO, QBO, BDC, solar cycle, and volcanic aerosols, and quantify the variances in the ERA5- and MERRA2-derived air mass and ozone STE monthly anomalies that can be explained by these interannual variabilities.

The annual-mean air mass STEs in the NH and SH extratropics and tropics from ERA5 are -12×10^9 kg s^{-1}, -10.5×10^9 kg s^{-1}, and 22.5×10^9 kg s^{-1}, respectively, the magnitudes of which are 12%, 2%, and 7% larger than the corresponding MERRA2 magnitudes of -10.7×10^9 kg s^{-1}, -10.3×10^9 kg s^{-1} and 21×10^9 kg s^{-1}. The annual-mean ozone STEs over the NH extratropics, SH extratropics, tropics, extratropics, and globe in the ERA5 are −342, −239, 201, −581, and −380 Tg year^{-1}, the magnitudes of which are 12%, 7%, 20%, 10%, and 5% larger than the corresponding MERRA2 magnitudes for −305, −224, 168, −529, −361 Tg year^{-1}. The annual-mean global ozone STE differences between ERA5 and MERRA2 are dominated by diabatic heating differences, compensated somewhat by ozone differences. The relative difference between ERA5 and MERRA2 in global ozone STE seasonal cycle is 40% in June and July and −40% in October and November, which is primarily due to difference in seasonal breathing of the lowermost stratosphere ozone mass (i.e., dM_{O_3}/dt).

The correlation coefficients between ERA5 and MERRA2 air mass STE monthly anomalies are 0.62, 0.45, and 0.37, respectively, over the NH and SH extratropics and tropics, corresponding to the variances of 38%, 20%, and 14% in the ERA5 and MERRA2 monthly anomalies that can be explained by each other. The correlation

coefficients between ERA5 and MERRA2 ozone STE monthly anomalies are 0.68, 0.34, 0.50, 0.46, and 0.57 in the NH extratropics, SH extratropics, tropics, extratropics, and globe, respectively, corresponding to the variances of 46%, 12%, 25%, 21%, and 33% in the ERA5 and MERRA2 monthly anomalies that can be explained by each other. It is also shown that relative differences in global ozone STE monthly anomalies between ERA5 and MERRA2 can be up to ±20%, which are mainly due to differences in ozone and dM_{O_3}/dt. The diabatic heating difference also plays a role.

The air mass and ozone STE interannual variabilities related to ENSO, QBO, BDC, solar cycle, and volcanic aerosols are examined. For the global ozone STE monthly anomalies, the variances that can be explained by ENSO, QBO, BDC, solar cycle, and volcanic aerosols are 5.0%–17.3%, 5.4%–7.2%, 1.0%–3.1%, 0.3%–1.8%, 7.0%–7.6%, respectively, with a residual variance 67.4%–76.9%. Similar results are obtained for ozone STE monthly anomalies over other regions. In addition, the volcanic aerosol impacts on ozone STEs from ERA5 and MERRA2 have opposite signs and thus are inconclusive.

Noting that ERA5 and MERRA2 can only explain each other's ozone STE monthly anomaly variance by 12%–46%, there must be large non-physical signals or errors in ERA5 and MERRA monthly anomalies. Caution is needed when using ERA5 and MERRA2 reanalyses to investigate the STE interannual variability. Future research is required to derive the air mass and ozone STEs based on observations, which could help understand the large discrepancies in STE seasonal cycle and especially monthly anomalies between ERA5 and MERRA2.

Data Availability Statement

The ERA5 data is downloaded from Copernicus Climate Change Service (C3S, 2017). The MERRA-2 data used in this study are available upon request from NASA Goddard Earth Sciences Data and Information Services Center (DISC) and described by Bosilovich et al. (2015).

Acknowledgments
This research was supported by NSF Grant AGS-2202812. Additional funding was provided by the Calvin Professorship in Atmospheric Sciences. We would like to acknowledge high-performance computing support from Cheyenne (https://doi.org/10.5065/D6RX99HX) provided by NCAR's Computational and Information Systems Laboratory, sponsored by the National Science Foundation, for the analyses presented in this study and for data management, storage, and preservation. We also wish to thank the International Space Science Institute (ISSI) Tropical Width Impacts on the Stratosphere (TWIST) group for the valuable discussions and feedback on this work.

References

Abalos, M., Calvo, N., Benito-Barca, S., Garny, H., Hardiman, S. C., Lin, P., et al. (2021). The Brewer–Dobson circulation in CMIP6. *Atmospheric Chemistry and Physics*, *21*(17), 13571–13591. https://doi.org/10.5194/acp-21-13571-2021

Abalos, M., Legras, B., Ploeger, F., & Randel, W. J. (2015). Evaluating the advective Brewer-Dobson circulation in three reanalyses for the period 1979–2012. *Journal of Geophysical Research: Atmospheres*, *120*(15), 7534–7554. https://doi.org/10.1002/2015JD023182

Abalos, M., Orbe, C., Kinnison, D. E., Plummer, D., Oman, L. D., Jöckel, P., et al. (2020). Future trends in stratosphere-to-troposphere transport in CCMI models. *Atmospheric Chemistry and Physics*, *20*(11), 6883–6901. https://doi.org/10.5194/acp-20-6883-2020

Abalos, M., Randel, W. J., Kinnison, D. E., & Serrano, E. (2013). Quantifying tracer transport in the tropical lower stratosphere using WACCM. *Atmospheric Chemistry and Physics*, *13*(21), 10591–10607. https://doi.org/10.5194/acp-13-10591-2013

Albers, J. R., Perlwitz, J., Butler, A. H., Birner, T., Kiladis, G. N., Lawrence, Z. D., et al. (2018). Mechanisms governing interannual variability of stratosphere-to-troposphere ozone transport. *Journal of Geophysical Research: Atmospheres*, *123*(1), 234–260. https://doi.org/10.1002/2017JD026890

Andrews, D. G., Leovy, C. B., & Holton, J. R. (1987). *Middle atmosphere dynamics*. Academic press.

Appenzeller, C., Holton, J. R., & Rosenlof, K. H. (1996). Seasonal variation of mass transport across the tropopause. *Journal of Geophysical Research*, *101*(D10), 15071–15078. https://doi.org/10.1029/96jd00821

Boothe, A. C., & Homeyer, C. R. (2017). Global large-scale stratosphere-troposphere exchange in modern reanalyses. *Atmospheric Chemistry and Physics*, *17*(9), 5537–5559. https://doi.org/10.5194/acp-17-5537-2017

Bosilovich, M. G., Lucchesi, R., & Suarez, M. (2015). Merra-2: File specification [Dataset]. GMAO Office Note No. 9 (Version 1.1). Retrieved from http://gmao.gsfc.nasa.gov/pubs/office_notes

Butchart, N. (2014). The Brewer-Dobson circulation. *Reviews of Geophysics*, *52*(2), 157–184. https://doi.org/10.1002/2013rg000448

Butchart, N., Scaife, A., Bourqui, M., De Grandpré, J., Hare, S., Kettleborough, J., et al. (2006). Simulations of anthropogenic change in the strength of the Brewer–Dobson circulation. *Climate Dynamics*, *27*(7–8), 727–741. https://doi.org/10.1007/s00382-006-0162-4

Collins, W. J., Derwent, R. G., Garnier, B., Johnson, C. E., Sanderson, M. G., & Stevenson, D. S. (2003). Effect of stratosphere-troposphere exchange on the future tropospheric ozone trend. *Journal of Geophysical Research*, *108*(D12), 8528. https://doi.org/10.1029/2002jd002617

Copernicus Climate Change Service (C3S). (2017). ERA5: Fifth generation of ECMWF atmospheric reanalyses of the global climate [Dataset]. Copernicus Climate Change Service Climate Data Store (CDS). Retrieved from https://cds.climate.copernicus.eu/#!/home

Duchon, C. E. (1979). Lanczos filtering in one and two dimensions. *Journal of Applied Meteorology and Climatology*, *18*(8), 1016–1022. https://doi.org/10.1175/1520-0450(1979)018<1016:lfioat>2.0.co;2

Fiore, A. M., Jacob, D. J., Field, B. D., Streets, D. G., Fernandes, S. D., & Jang, C. (2002). Linking ozone pollution and climate change: The case for controlling methane. *Geophysical Research Letters*, *29*(19), 25-1–25-4. https://doi.org/10.1029/2002gl015601

Fu, Q., Lin, P., Solomon, S., & Hartmann, D. (2015). Observational evidence of strengthening of the Brewer-Dobson circulation since 1980. *Journal of Geophysical Research: Atmospheres*, *120*(19), 10214–10228. https://doi.org/10.1002/2015jd023657

Fu, Q., Solomon, S., & Lin, P. (2010). On the seasonal dependence of tropical lower-stratospheric temperature trends. *Atmospheric Chemistry and Physics*, *10*(6), 2643–2653. https://doi.org/10.5194/acp-10-2643-2010

Fu, Q., Solomon, S., Pahlavan, H. A., & Lin, P. (2019). Observed changes in Brewer–Dobson circulation for 1980–2018. *Environmental Research Letters*, *14*(11), 114026. https://doi.org/10.1088/1748-9326/ab4de7

Fu, Q., Wang, M., White, R. H., Pahlavan, H. A., Alexander, B., & Wallace, J. M. (2020a). Quasi-Biennial oscillation and sudden stratospheric warmings during the Last Glacial Maximum. *Atmosphere-Basel*, *11*(9), 943. https://doi.org/10.3390/atmos11090943

Fu, Q., White, R. H., Wang, M., Alexander, B., Solomon, S., Gettelman, A., et al. (2020). The Brewer-Dobson circulation during the Last Glacial Maximum. *Geophysical Research Letters*, *47*(5), e2019GL086271. https://doi.org/10.1029/2019gl086271

Fujiwara, M., Manney, G. L., Gray, L. J., Wright, J. S., Tegtmeier, S., Ivanciu, I., & Pilch Kedzierski, R. (2022). SPARC reanalysis intercomparison project (S-RIP) final report.

Gelaro, R., McCarty, W., Suárez, M. J., Todling, R., Molod, A., Takacs, L., et al. (2017). The modern-era retrospective analysis for research and applications, version 2 (MERRA-2). *Journal of Climate*, *30*(14), 5419–5454. https://doi.org/10.1175/jcli-d-16-0758.1

Geng, L., Murray, L. T., Mickley, L. J., Lin, P., Fu, Q., Schauer, A. J., & Alexander, B. (2017). Isotopic evidence of multiple controls on atmospheric oxidants over climate transitions. *Nature*, *546*(7656), 133–+. https://doi.org/10.1038/nature22340

Gettelman, A., Holton, J. R., & Rosenlof, K. H. (1997). Mass fluxes of O_3, CH_4, N_2O and CF_2Cl_2 in the lower stratosphere calculated from observational data. *Journal of Geophysical Research*, *102*(D15), 19149–19159. https://doi.org/10.1029/97jd01014

Hegglin, M. I., & Shepherd, T. G. (2009). Large climate-induced changes in ultraviolet index and stratosphere-to-troposphere ozone flux. *Nature Geoscience*, *2*(10), 687–691. https://doi.org/10.1038/ngeo604

Hersbach, H., Bell, B., Berrisford, P., Hirahara, S., Horányi, A., Muñoz-Sabater, J., et al. (2020). The ERA5 global reanalysis. *The Quarterly Journal of the Royal Meteorological Society*, *146*(730), 1999–2049. https://doi.org/10.1002/qj.3803

Hess, P., Kinnison, D., & Tang, Q. (2015). Ensemble simulations of the role of the stratosphere in the attribution of northern extratropical tropospheric ozone variability. *Atmospheric Chemistry and Physics*, *15*(5), 2341–2365. https://doi.org/10.5194/acp-15-2341-2015

Holton, J. R., Haynes, P. H., McIntyre, M. E., Douglass, A. R., Rood, R. B., & Pfister, L. (1995). Stratosphere-troposphere exchange. *Reviews of Geophysics*, *33*(4), 403–439. https://doi.org/10.1029/95RG02097

Hsu, J., & Prather, M. J. (2009). Stratospheric variability and tropospheric ozone. *Journal of Geophysical Research*, *114*(D6), D06102. https://doi.org/10.1029/2008JD010942

Hsu, J., Prather, M. J., & Wild, O. (2005). Diagnosing the stratosphere-to-troposphere flux of ozone in a chemistry transport model. *Journal of Geophysical Research*, *110*(D19), D19305. https://doi.org/10.1029/2005jd006045

Hsu, J. N., & Prather, M. J. (2014). Is the residual vertical velocity a good proxy for stratosphere-troposphere exchange of ozone? *Geophysical Research Letters*, *41*(24), 9024–9032. https://doi.org/10.1002/2014gl061994

Kentarchos, A. S., & Roelofs, G. J. (2003). A model study of stratospheric ozone in the troposphere and its contribution to tropospheric OH formation. *Journal of Geophysical Research*, *108*(D12), 8517. https://doi.org/10.1029/2002JD002598

Li, F., Austin, J., & Wilson, J. (2008). The strength of the Brewer-Dobson circulation in a changing climate: Coupled chemistry-climate model simulations. *Journal of Climate*, *21*(1), 40–57. https://doi.org/10.1175/2007jcli1663.1

Li, Y., & Thompson, D. W. J. (2013). The signature of the stratospheric Brewer–Dobson circulation in tropospheric clouds. *Journal of Geophysical Research: Atmospheres*, *118*(9), 3486–3494. https://doi.org/10.1002/jgrd.50339

Lin, M. Y., Fiore, A. M., Horowitz, L. W., Langford, A. O., Oltmans, S. J., Tarasick, D., & Rieder, H. E. (2015). Climate variability modulates western US ozone air quality in spring via deep stratospheric intrusions. *Nature Communications*, *6*(1), 7105. https://doi.org/10.1038/ncomms8105

Lin, P., & Fu, Q. (2013). Changes in various branches of the Brewer-Dobson circulation from an ensemble of chemistry climate models. *J Geophys Res-Atmos*, *118*(1), 73–84. https://doi.org/10.1029/2012jd018813

Lin, P., Fu, Q., Solomon, S., & Wallace, J. M. (2009). Temperature trend patterns in Southern Hemisphere high latitudes: Novel indicators of stratospheric change. *Journal of Climate*, *22*(23), 6325–6341. https://doi.org/10.1175/2009JCLI2971.1

Lindeman, R. H. (1980). Introduction to bivariate and multivariate analysis*Rep*.

Lu, H., Scaife, A. A., Marshall, G. J., Turner, J., & Gray, L. J. (2017). Downward wave reflection as a mechanism for the stratosphere–troposphere response to the 11-yr solar cycle. *Journal of Climate*, *30*(7), 2395–2414. https://doi.org/10.1175/JCLI-D-16-0400.1

Meul, S., Langematz, U., Kröger, P., Oberländer-Hayn, S., & Jöckel, P. (2018). Future changes in the stratosphere-to-troposphere ozone mass flux and the contribution from climate change and ozone recovery. *Atmospheric Chemistry and Physics*, *18*(10), 7721–7738. https://doi.org/10.5194/acp-18-7721-2018

Murphy, D. M., & Fahey, D. W. (1994). An estimate of the flux of stratospheric reactive nitrogen and ozone into the troposphere. *Journal of Geophysical Research*, *99*(D3), 5325–5332. https://doi.org/10.1029/93jd03558

Olaguer, E. P., Yang, H., & Tung, K. K. (1992). A reexamination of the radiative balance of the stratosphere. *Journal of the Atmospheric Sciences*, *49*(14), 1242–1263. https://doi.org/10.1175/1520-0469(1992)049<1242:Arotrb>2.0.Co;2

Olsen, M. A., Douglass, A. R., & Kaplan, T. B. (2013). Variability of extratropical ozone stratosphere-troposphere exchange using microwave limb sounder observations. *J Geophys Res-Atmos*, *118*(2), 1090–1099. https://doi.org/10.1029/2012jd018465

Olsen, M. A., Schoeberl, M. R., & Douglass, A. R. (2004). Stratosphere-troposphere exchange of mass and ozone. *Journal of Geophysical Research*, *109*(D24), D24114. https://doi.org/10.1029/2004jd005186

Olsen, S. C., McLinden, C. A., & Prather, M. J. (2001). Stratospheric N_2O-NOy system: Testing uncertainties in a three-dimensional framework. *Journal of Geophysical Research*, *106*(D22), 28771–28784. https://doi.org/10.1029/2001jd000559

Ordonez, C., Brunner, D., Staehelin, J., Hadjinicolaou, P., Pyle, J. A., Jonas, M., et al. (2007). Strong influence of lowermost stratospheric ozone on lower tropospheric background ozone changes over Europe. *Geophysical Research Letters*, *34*(7), L07805. https://doi.org/10.1029/2006gl029113

Pahlavan, H. A., Fu, Q., Wallace, J. M., & Kiladis, G. N. (2021). Revisiting the quasi-biennial oscillation as seen in ERA5. Part I: Description and momentum budget. *Journal of the Atmospheric Sciences*, *78*(3), 673–691. https://doi.org/10.1175/jas-d-20-0248.1

Roelofs, G.-J., & Lelieveld, J. (1997). Model study of the influence of cross-tropopause O_3 transports on tropospheric O_3 levels. *Tellus B: Chemical and Physical Meteorology*, *49*(1), 38–55. https://doi.org/10.3402/tellusb.v49i1.15949

Rosenlof, K. H. (1995). Seasonal cycle of the residual mean meridional circulation in the stratosphere. *Journal of Geophysical Research*, *100*(D3), 5173–5191. https://doi.org/10.1029/94jd03122

Rosenlof, K. H., & Holton, J. R. (1993). Estimates of the stratospheric residual circulation using the downward control principle. *Journal of Geophysical Research*, *98*(D6), 10465–10479. https://doi.org/10.1029/93jd00392

Ruiz, D. J., & Prather, M. J. (2022). From the middle stratosphere to the surface, using nitrous oxide to constrain the stratosphere–troposphere exchange of ozone. *Atmospheric Chemistry and Physics*, *22*(3), 2079–2093. https://doi.org/10.5194/acp-22-2079-2022

Santer, B. D., Wigley, T. M. L., Boyle, J. S., Gaffen, D. J., Hnilo, J. J., Nychka, D., et al. (2000). Statistical significance of trends and trend differences in layer-average atmospheric temperature time series. *Journal of Geophysical Research*, *105*(D6), 7337–7356. https://doi.org/10.1029/1999JD901105

Sato, M., Hansen, J. E., McCormick, M. P., & Pollack, J. B. (1993). Stratospheric aerosol optical depths, 1850–1990. *Journal of Geophysical Research*, *98*(D12), 22987–22994. https://doi.org/10.1029/93JD02553

Schoeberl, M. R. (2004). Extratropical stratosphere-troposphere mass exchange. *Journal of Geophysical Research*, *109*(D13), D13303. https://doi.org/10.1029/2004jd004525

Seidel, D. J., Li, J., Mears, C., Moradi, I., Nash, J., Randel, W. J., et al. (2016). Stratospheric temperature changes during the satellite era. *Journal of Geophysical Research: Atmospheres*, *121*(2), 664–681. https://doi.org/10.1002/2015JD024039

Škerlak, B., Sprenger, M., & Wernli, H. (2014). A global climatology of stratosphere–troposphere exchange using the ERA-Interim data set from 1979 to 2011. *Atmospheric Chemistry and Physics*, *14*(2), 913–937. https://doi.org/10.5194/acp-14-913-2014

Stohl, A., Bonasoni, P., Cristofanelli, P., Collins, W., Feichter, J., Frank, A., et al. (2003). Stratosphere-troposphere exchange: A review, and what we have learned from STACCATO. *Journal of Geophysical Research*, *108*(D12), 8516. https://doi.org/10.1029/2002jd002490

Sweeney, A., Fu, Q., Pahlavan, H. A., & Haynes, P. (2023). Seasonality of the QBO impact on equatorial clouds. *Journal of Geophysical Research: Atmospheres*, *128*(7), e2022JD037737. https://doi.org/10.1029/2022JD037737

Sweeney, A. J., & Fu, Q. (2023). Interannual variability of temperature, water vapor, and clouds in the tropical tropopause layer. *ESS Open Archive*. https://doi.org/10.22541/essoar.168167390.09887630/v1

Tapping, K. F., & Morton, D. C. (2013). The next generation of Canadian solar flux monitoring. *Paper presented at IOP publishing journal of physics: Conference series*.

Tie, X., & Hess, P. (1997). Ozone mass exchange between the stratosphere and troposphere for background and volcanic sulfate aerosol conditions. *Journal of Geophysical Research*, *102*(D21), 25487–25500. https://doi.org/10.1029/97JD01842

Ueyama, R., & Wallace, J. M. (2010). To what extent does high-latitude wave forcing drive tropical upwelling in the Brewer–Dobson circulation? *Journal of the Atmospheric Sciences*, *67*(4), 1232–1246. https://doi.org/10.1175/2009JAS3216.1

Wang, M., & Fu, Q. (2021). Stratosphere-troposphere exchange of air masses and ozone concentrations based on reanalyses and observations. *Journal of Geophysical Research: Atmospheres*, *126*(18). e2021JD035159. https://doi.org/10.1029/2021jd035159

Wang, M., & Fu, Q. (2023). Changes in stratosphere-troposphere exchange of air mass and ozone concentration in CCMI Models from 1960-2099. *Journal of Geophysical Research: Atmospheres*, *128*(13), e2023JD038487. https://doi.org/10.1029/2023jd038487

Wang, M., Fu, Q., Solomon, S., Alexander, B., & White, R. H. (2022). Stratosphere-troposphere exchanges of air mass and ozone concentration in the Last Glacial Maximum. *Journal of Geophysical Research: Atmospheres*, *127*(10), e2021JD036327. https://doi.org/10.1029/2021JD036327

Wang, M., Fu, Q., Solomon, S., White, R. H., & Alexander, B. (2020). Stratospheric ozone in the Last Glacial Maximum. *Journal of Geophysical Research: Atmospheres*, *125*(21), e2020JD032929. https://doi.org/10.1029/2020jd032929

WMO. (2010). *Scientific assessment of ozone depletion*. Global Ozone Research and Monitoring Project, Report No. 52, 2011.

Wolter, K., & Timlin, M. S. (2011). El Niño/Southern Oscillation behaviour since 1871 as diagnosed in an extended multivariate ENSO index (MEI.ext). *International Journal of Climatology*, *31*(7), 1074–1087. https://doi.org/10.1002/joc.2336

Woollings, T., Drouard, M., O'Reilly, C. H., Sexton, D. M. H., & McSweeney, C. (2023). Trends in the atmospheric jet streams are emerging in observations and could be linked to tropical warming. *Communications Earth & Environment*, *4*(1), 125. https://doi.org/10.1038/s43247-023-00792-8

Yang, H., Chen, G., Tang, Q., & Hess, P. (2016). Quantifying isentropic stratosphere-troposphere exchange of ozone. *Journal of Geophysical Research: Atmospheres*, *121*(7), 3372–3387. https://doi.org/10.1002/2015JD024180

Zeng, G., & Pyle, J. A. (2005). Influence of El Niño Southern Oscillation on stratosphere/troposphere exchange and the global tropospheric ozone budget. *Geophysical Research Letters*, *32*(1), L01814. https://doi.org/10.1029/2004GL021353